Inorganic Chemistry

Article

pubs.acs.org/IC

Two Novel Ternary Dicopper(II) μ-Guanazole Complexes with Aromatic Amines Strongly Activated by Quantum Dots for DNA Cleavage

Javier Hernández-Gil,[†,○] Sacramento Ferrer,*[,†] Alfonso Castiñeiras,[‡] Malva Liu-González,[§] Francesc Lloret,[∥] Ángela Ribes,[†] Lucija Čoga,[†] Anja Bernecker,[⊥] and Juan C. Mareque-Rivas*[,⊥,#,▽]

[†]Departament de Química Inorgànica, Universitat de València, Vicent Andrés Estellés s/n, 46100 Burjassot, Valencia, Spain

[‡]Departamento de Química Inorgánica, Universidad de Santiago de Compostela, Campus Universitario Sur, E-15782 Santiago de Compostela, Spain

[§]S.C.S.I.E., Universitat de València, Dr. Moliner 50, 46100 Burjassot, Valencia, Spain

[∥]Institut de Ciència Molecular, Universitat de València, Catedràtic José Beltrán n° 2, 46980 Paterna, Valencia, Spain

[⊥]Cooperative Centre for Research in Biomaterials (CIC biomaGUNE), 20009 San Sebastián, Spain

[#]IKERBASQUE, Basque Foundation for Science, 48011 Bilbao, Spain

[▽]Departmento de Bioquimica y Biologia Molecular, Universidad del Pais Vasco, 48940 Leioa, Spain

Supporting Information

ABSTRACT: Two novel (μ-guanazole)-bridged binuclear copper(II) complexes with 1,10-phenanthroline (phen) or 2,2′-bipyridine (bipy), $[Cu_2(\mu\text{-}N2,N4\text{-Hdatrz})(phen)_2(H_2O)(NO_3)_4]$ (**1**) and $[Cu_2(\mu\text{-}N1,N2\text{-datrz})_2(\mu\text{-}OH_2)(bipy)_2](ClO_4)_2$ (**2**) (Hdatrz = 3,5-diamino-1,2,4-triazole = guanazole), have been prepared and characterized by X-ray diffraction, spectroscopy, and susceptibility measurements. Compounds **1** and **2** differ in the aromatic amine, which acts as a coligand, and in the Cu···Cu′-bridging system. Compound **1**, which contains two mono-bridged copper ions, represents the first example of a discrete Cu−(*NCN*-trz)−Cu′ complex. Compound **2**, with two triply bridged copper ions, is one of the few compounds featuring a Cu−[(*NN*-trz)$_2$ + (*O*-aquo)]−Cu′ unit. Both compounds display antiferromagnetic coupling but of different magnitude: J ($\mu_{2,4}$-triazole) = −52 cm^{-1} for **1** and J ($\mu_{1,2}$-triazolate) = −115 cm^{-1} for **2**. The DNA binding and cleavage properties of the two compounds have been investigated. Fluorescence, viscosimetry, and thermal denaturation studies reveal that both complexes have high affinity for DNA (**1** > **2**) and that only **1** acts as an intercalator. In the presence of a reducing agent like 3-mercaptopropionic acid, **1** produces significant oxidative DNA cleavage, whereas **2** is inactive. However, in the presence of very small quantities of micelles filled with core−shell CdSe-ZnS quantum dots (15 nM), **1** and **2** are considerably more active and become highly efficient nucleases as a result of the different possible mechanisms for promoting cooperative catalysis (metal−metal, metal−hydrogen bonding, metal−intercalation, and metal−nanoparticle). Electrophoresis DNA-cleavage inhibition experiments, X-ray photoelectron spectroscopy studies, and fluorescence ethidium bromide displacement assays reveal that in these novel nucleases the QDs act as redox-active protein-like nanoparticle structures that bind to the DNA and deliver electrons to the copper(II) centers for the generation of Cu(I) and reactive oxygen species.

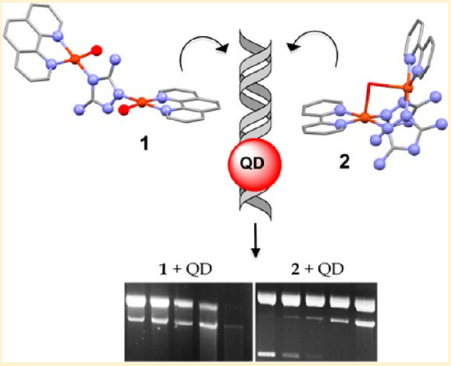

INTRODUCTION

In recent years, different types of inorganic nanoparticles (iNPs) with unique physicochemical properties have emerged.[1−4] Among these, quantum dots (QDs) have proved to be very versatile, finding applications in electroluminescent displays,[5] quantum computing,[6] photovoltaics,[7] solar cells,[8] solid-state lighting,[9] transistors,[10] and biological imaging.[11,12] The useful physicochemical properties of QDs include their broad excitation bands with very high extinction coefficients and narrow emission bands that can be tuned across a region of the visible or near-infrared spectrum by varying the size and composition of the QD with high photostability. For biological imaging applications, QDs are now excellent alternatives to organic chromophores.[11,12] In catalysis-involving redox processes, QDs have also become the focus of increasing interest by showing the capacity to deliver multiple electrons upon irradiation with light.[13,14]

In addition to interesting properties arising from the semiconductor nanocrystal, it has been reported that the surface of water-soluble QDs can readily adsorb oligonucleotides and various serum albumins.[15,16] Moreover, recent observations suggest that there may be functional similarities between NPs and proteins,[17−20] given that they can have similar sizes, shapes, and surface functional groups. In this context, some studies

Received: October 31, 2013
Published: December 12, 2013

have shown that nanosized QDs can be considered generic curved surfaces that DNA can wrap around.[18−20] This is important because bending may open and close certain sites along the double helix, making certain regions of the DNA more or less accessible. Potentially, this could have widespread implications and applications because it could lead to artificial regulation of a wide array of cellular processes for therapeutic and biotechnological applications, much like protein−DNA interactions do naturally.[21] In addition to enabling different applications, the effects of DNA−QD interactions need to be considered also from a toxicological point of view. However, there are contradictory reports concerning the ability of QDs to damage DNA in the absence and presence of light as well as their toxicity to cells.[22−26]

A potentially prolific new direction in inorganic chemistry and nanochemistry could be to combine NPs with small metal complexes to seek synergistic and/or cooperative effects. In this context, combining QDs with coordination complexes is being explored as a new strategy to obtain cooperative systems with improved properties for applications in catalysis for solar-energy conversion,[14,27−29] receptor chemistry and sensing,[30−34] biological imaging,[35,36] and molecular therapy.[37−40]

A prominent area of research in coordination chemistry is the development of metal complexes that can act as artificial nucleases. Overall, these synthetic DNA-cleaving reagents operate using one of two distinct mechanisms: (i) oxidative scission of deoxyribose residues through redox chemistry[41] and (ii) hydrolysis of the phosphodiester sugar backbone.[42] The most classical example of oxidative DNA-cleavage activity is exemplified by the Cu(II)-1,10-phenanthroline (1,10-phenanthroline = phen) system, which has been utilized as a footprinting reagent for the evaluation of protein−DNA interactions as well as a probe for DNA and RNA secondary structure.[43−48] In this intensively investigated system, $[Cu(phen)_2]^+$ generated in the presence of a reducing agent and molecular oxygen afford activated oxygen species for DNA cleavage, whereas the intercalation of phen into the DNA minor groove allows for DNA targeting. Recently, we discovered that QDs cooperate and synergize with the Cu(II)-1,10-phenanthroline system for DNA cleavage, providing both the first example of cooperative DNA cleavage between NPs and a small-molecule-based synthetic metallonuclease and a potentially new approach to develop more efficient DNA-cleaving systems.[49]

Many ligand systems and approaches have been tested with varying degrees of success to increase both the DNA scission capability and the affinity of copper metallonucleases for DNA.[41] A popular strategy is to use bimetallic agents because of the potential cooperative effects that can arise between the two metal centers. However, an emerging way to design more powerful synthetic catalysts for a wide range of transformations, including DNA cleavage, utilizes ligands with hydrogen-bonding features resembling those found in the active sites of metalloenzymes.[50−69]

In this Article, we have combined the advantages of dinuclear copper catalysts with those of hydrogen-bonding ligands, and we exploit QDs as a redox-active protein-like nanostructure to activate strongly the copper catalysts for DNA cleavage. Two mono(phen)-Cu^{II} fragments have been attached in the same compound by means of a single μ-triazole bridge using the ligand guanazole (guanazole= 3,5-diamino-1,2,4-triazole = Hdatrz, Scheme 1), thus yielding two copper centers with labile coordination sites of facile substitution and a structure suitable for DNA intercalation. The analogous bipy (2,2′-bipyridine = bipy)

Scheme 1

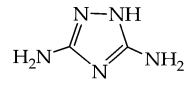

Hdatrz

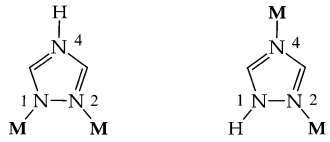

*N*1,*N*2 bridging mode *N*2,*N*4 bridging mode

ternary compound was been prepared, resulting in a dinuclear compound that contains a bis(guanazolate) bridge. In addition to providing a bridge between the two copper centers, the X-ray crystal structures reveal that the guanazole/guanazolato provides N−H groups for hydrogen-bonding interactions with the DNA. To effect DNA cleavage efficiently, these new copper complexes are combined with water-soluble micelles filled with CdSe-ZnS core−shell QDs.

We describe herein the synthesis, crystal structure, and magnetic properties of the two dinuclear copper complexes: $[\{Cu(phen)(H_2O)(NO_3)_2\}_2(\mu\text{-}N2,N4\text{-Hdatrz})]$ or $[Cu_2(\mu\text{-Hdatrz})(phen)_2(H_2O)_2(NO_3)_4]$ (**1**) (Hdatrz = guanazole = 3,5-diamino-1,2,4-triazole) and $[\{Cu(bipy)\}_2(\mu\text{-}N1,N2\text{-datrz})_2(\mu\text{-}OH_2)](ClO_4)_2$ or $[Cu_2(\mu\text{-datrz})_2(\mu\text{-}OH_2)(bipy)_2](ClO_4)_2$ (**2**). We report that these new copper complexes acting as nucleases are strongly activated in the presence of QD-filled micelles (MQDs) even in the absence of light. Then, different techniques were applied to investigate the functional role of the QD in this process.

EXPERIMENTAL SECTION

Materials and Chemicals. The ligand, guanazole, and copper salts were supplied by Sigma. Biological reagents: Plasmid pUC18 (0.5 μg/μL, 750 μM in nucleotides) in TE (Tris 10 mM and EDTA 1 mM, pH 8.0) buffer was purchased from Fermentas. Calf thymus DNA (CT-DNA), type XV, was obtained from Sigma. The rest of the reagents and chemicals were obtained from commercial sources and used without further purification.

Instrumentation and Methods. Elemental analyses were performed with a CE Instrument EA 1110 CHNS analyzer. Infrared spectra were recorded as KBr disks using a Mattson Satellite FTIR spectrophotometer from 4000 to 400 cm^{-1}. Low-resolution electrospray ionization mass spectrometry (ESI-MS) analysis in positive mode was performed on a Bruker Esquire 3000 plus LC−MS system; high-resolution ESI-MS in positive mode was performed on an ABS Giex Triple TOF 5600 or on a Waters LCT Premier XE. Magnetic susceptibility measurements on polycrystalline samples were carried out with a superconducting quantum interference design (SQUID) magnetometer in the temperature range 1.9−300 K. Diamagnetic corrections of the constituent atoms were estimated from Pascal's constants. Experimental susceptibilities were also corrected for the temperature-independent paramagnetism [60×10^{-6} cm^3 mol^{-1} per copper(II)] and for the magnetization of the sample holder. Transmision electron microscopy (TEM) studies were conducted on a JEOL JEM-2011 electron microscope operating at 200 kV. The sample was prepared by depositing a drop of a solution of nanocrystal onto a copper specimen grid coated with a holey ultrathin carbon film and allowing it to dry. Dynamic light scattering measurements were measured with a NanoSizer (Malvern Nano-Zs, UK).

Synthesis of $[Cu_2(\mu\text{-Hdatrz})(phen)_2(H_2O)_2(NO_3)_4]$ *(**1**).* An aqueous solution of $Cu(NO_3)_2{\cdot}2.5H_2O$ (1.148 g, 5 mmol, 20 mL) was mixed with an aqueous solution of guanazole (0.248 g, 2.5 mmol, 5 mL).

dx.doi.org/10.1021/ic4027249 | *Inorg. Chem.* 2014, 53, 578−593

A green solution was formed to which an aqueous suspension of phenantroline·H_2O (0.993 g, 5 mmol, 10 mL) was added dropwise. A dark turbidity was almost immediately observed. After 2 h of stirring, a black−green precipitate was filtered off, and the resulting dark green solution was allowed to stand at room temperature covered with Parafilm. Within ca. 1 month, a few large black−green crystals, not suitable for X-ray, appeared; they were separated by filtration. From the remaining solution, after ca. 2 months, smaller green crystals of **1** came out, which were collected by filtration, washed with water, and dried in air. Yield (on green crystals, corresponding to **1**): ca. 650 mg (ca. 30%). Microanalysis performed on these crystals: Calcd for $C_{26}H_{25}Cu_2N_{13}O_{14}$ (870.67): C, 35.87; H, 2.89; N, 20.91. Found: C, 35.74; H, 2.87; N, 20.81. FT-IR (**1**, green crystals) (KBr pellet) $\tilde{\nu}_{max}$ (cm^{-1}): 3318m [$\upsilon(O-H)_{H_2O}$ + $\nu(N-H)_{NH,NH_2}$], 1640m + 1585w [υ(C=N)/ring st + $\delta(N-H)_{NH,NH_2}]_{gua}$, 1519m + 1496w + 1427sh [υ(C=N)/ring st]$_{phen}$, 1385vs [$\upsilon_a(NO_2)$], 1312m [$\upsilon_s(NO_2)$], 852m + 721m [δ_{oop}(arC-H)]$_{phen}$. E.A and IR of black and green crystals (**1**) are almost coincident but not identical.

*Synthesis of [$Cu_2(\mu$-datrz$)_2(\mu$-$OH_2)$(bipy$)_2$](ClO$_4)_2$ (**2**).* An aqueous suspension of bipy (0.156 g, 1 mmol, 20 mL) was slowly added (drop by drop) to an equimolar aqueous solution of $Cu(ClO_4)_2·6H_2O$ (0.37 g, 1 mmol, 20 mL). To this mixture, an aqueous solution of guanazole (0.02 g, 0.25 mmol, 5 mL) was slowly added. The reaction mixture was stirred for 2 h. A light blue precipitate was formed and filtered off. The remaining dark green solution was allowed to stand at room temperature. After 1 day, dark green single crystals of **2** appeared. Yield (on green crystals, corresponding to **2**): 30 mg (14%). Microanalysis (performed on single crystals): Calcd for $C_{24}H_{26}Cu_2N_{14}O_9Cl_2$ (852.57): C, 33.81; H, 3.07; N, 23.00. Found: C, 33.60; H, 3.12; N, 23.15. FT-IR (**2**, green crystals) (KBr pellet) $\tilde{\nu}_{max}$ (cm^{-1}): 3386b,s [$\upsilon(O-H)_{H_2O}$ + $\delta(N-H)_{NH_2}$], 1656sh + 1618m + 1561m + 1509 + 1499d,m + 1447m [υ(C=N)/ring st + $\nu(N-H)_{NH_2}$], 1121vs + 1090s [$\upsilon_a(ClO_4)$], 769w [$\upsilon_s(ClO_4)$]. IR of blue precipitate corresponds to a binary Cu-bipy-ClO^-_4 compound.

Synthesis of Micelles Filled with QDs and SPIONs. Micelles core−shell CdSe-ZnS QD were synthesized, characterized, and purified as described previously.[49,70,71] The CdSe-ZnS QD have an average diameter of 5.2 nm (4.0 nm CdSe core diameter and 0.6 nm ZnS shell thickness). The results reported in this study are for nanocrystals that have the first absorption band at 600 nm and a maximum emission peak at 645 nm.

The MQDs were prepared by self-assembly process of PEGylated phospholipids around hydrophobic CdSe-ZnS core−shell QDs.[71] The water-soluble micelles with encapsulated superparamagnetic iron oxide nanoparticles of 6 nm as core material were prepared in the same way.[72]

X-ray Crystallography. A green prismatic crystal of **1** and dark green crystal of **2** were mounted on a glass fiber and used for data collection. Crystal data were collected at 293(2) K using a Bruker X8 Kappa APEXII diffractometer. Graphite monochromated Mo Kα radiation (λ = 0.71073 Å) was used throughout. The data were processed with APEX2.[73] The structure was solved by direct methods using the program SHELXS-97[74] and refined by full-matrix least-squares techniques againts F^2 using SHELXL-97.[74] Positional and anisotropic atomic displacement parameters were refined for all nonhydrogen atoms. Hydrogen atoms attached to carbon and nitrogen atoms were placed in geometrically idealized positions and refined using a riding model. Hydrogen atoms on water molecules were located from difference Fourier maps and were also refined using a riding model. Some problem of disorder in the NO_3 (**1**)/ClO_4 (**2**) groups gave rise to rather high U_{eq}. Criteria of a satisfactory complete analysis were the ratios of rms shift to standard deviation less than 0.001 and no significant features in final difference maps. Atomic scattering factors were from the International Tables for Crystallography.[75] Molecular graphics were from DIAMOND.[76] The details of crystallographic data and structure refinements parameters for complexes **1** and **2** are summarized in Table 1. Cambridge Crystallographic Data Centre (CCDC) file nos. 901545 (**1**) and 912352 (**2**) contain the crystallographic data for this Article. These data can be obtained free of charge from The CCDC at www.ccdc.cam.ac.uk/data_request/cif. Crystallographic literature revision was performed with the help of CSD-Conquest.[77]

Table 1. Crystallographic Data for Complexes 1 and 2

parameter	1	2
empirical formula	$C_{26}H_{25}Cu_2N_{13}O_{14}$	$C_{24}H_{26}Cl_2Cu_2N_{14}O_9$
formula weight	870.67	852.57
crystal system	triclinic	monoclinic
space group	$P\bar{1}$	$P2_1/c$
temperature (K)	293(2)	293(2)
wavelength (Å)	0.71069	0.71703
a (Å)	10.725(5)	16.2221(7)
b (Å)	12.310(5)	13.9144(7)
c (Å)	14.278(5)	15.4530(5)
α (degrees)	103.673(5)	90
β (degrees)	102.037(5)	109.799(2)
γ (degrees)	108.806(5)	90
V (Å^3)	1648.7(12)	3281.9
Z	2	4
density (M g^{-3})	1.754	1.726
Abs coeff. (mm^{-1})	1.381	1.533
Abs correction	semiempirical from equiv	semiempirical from equiv
F (000)	884	1728
total no. of reflections	9696	12 830
reflections, $I > 2\sigma(I)$	6476	7425
θ range for data collection (degrees)	1.54 to 25.98	1.33 to 27.44
ranges (h, k, l)	$-12 \le h \le 13$	$-21 \le h \le 21$
	$-15 \le k \le 15$	$-17 \le k \le 16$
	$-17 \le l \le 17$	$-20 \le h \le 20$
completeness to θ (%)	98.8	99.2
refinement method	full-matrix least-squares on F^2	full-matrix least-squares on F^2
goodness-of-fit on F^2	1.078	1.083
R indices [$I > 2\sigma(I)$]	0.0603	0.0500
R indices (all data)	0.0921	0.0801

DNA−Copper Complex Interaction Studies. The fluorescence spectra were recorded with a JASCO FP-6200 spectrofluorometer at room temperature. Ethidium bromide (EB) was used as a reference to determine the relative DNA-binding properties of complexes **1** and **2** to calf thymus (CT-DNA). The experiments entailed the addition of copper(II) complex solutions at final concentrations ranging from 0 to 50 μM to samples containing 50 μM base pairs CT-DNA and 50 μM EB in cacodylate buffer (0.1 M, pH 6.0). All of the samples were excited at 500 nm, and emission was recorded between 530 and 650 nm.

For competitive ethidium-displacement assays, the experiments were carried out by adding serial aliquots of the different complexes into a solution containing 3 μM CT-DNA (ε_{260} = 13 200 M $bp^{-1}cm^{-1}$) and 3.78 μM EB in cacodylate buffer (0.1 M, pH 6.0) until 50% of the initial fluorescence was lost. Complexes **1** and **2** stock solutions were prepared at 0.5 mM in cacodylate buffer (0.1 M, pH 6.0). Excitation and emission wavelengths were set to 500 and 595 nm, respectively. The apparent binding constants were calculated using $K_{app} = K_{EB} \times (3.78/C_{50})$ where $K_{EB} = 3 \times 10^7$ M bp^{-1}. This K_{EB} value (pH 6.0) was calculated by following literature procedures.[78−80] To study the influence of MQD in the DNA affinity of the complexes, an aliquot of MQD (final concentration of 30 nM) was added to the solution CT-DNA-EB (3 μM CT-DNA and 3.78 μM EB). After equilibration for 15−20 min, an aliquot of **1** (or **2**) was added to the mixture until 50% of the fluorescence was lost.

For QD−CT-DNA interaction studies, a working solution containing 600 nM QD in cacodylate buffer (0.1 M, pH 6.0) was prepared. The experiment entailed the addition of serial aliquots of a CT-DNA stock solution. After each addition, the samples were excited at 400 nm, and emission was recorded between 580 and 700 nm.

dx.doi.org/10.1021/ic4027249 | Inorg. Chem. 2014, 53, 578−593

DNA-melting experiments were carried out by monitoring the absorbance spectrum between 1000 and 200 nm of CT-DNA (100 μM bp) at different temperatures both in the absence and presence of complexes **1** and **2** in a ratio of 4:1 [DNA]/[complex]. Measurements were carried out with an Agilent 8453 UV−vis spectrophotometer equipped with a Peltier temperature-controlled sample cell and driver (Agilent 89090A). The solution containing the complex and CT-DNA in phosphate buffer (1 mM phosphate, 2 mM NaCl, pH 7.2) was stirred continuously and heated with a temperature increase rate of 1 °C min^{-1}. The temperature interval studied ranged from 25 to 90 °C. The melting point was obtained with the first derivative.

Viscosity measurements were carried out using a semimicro Ubbelohde viscosimeter maintained at a constant temperature of 25.0 ± 0.1 °C in a Julabo ME16G thermostatic bath. Solutions of complexes **1** and **2** (final concentrations ranging from 1 to 10 μM) in cacodylate buffer (0.1 M, pH 6.0) were added to a solution of 50 μM bp CT-DNA in the same buffer. The flow times were measured in triplicate with a stopwatch. Data were presented as $(\eta/\eta_0)^{1/3}$ versus the ratio of the complex concentration to DNA, where η is the viscosity of the DNA in the presence of the complex and η_0 is the viscosity of the DNA alone. Viscosity values were calculated from the observed flow time of a DNA-containing solution corrected for the flow time of buffer alone (t_0), $\eta = t - t_0$.

DNA-Cleavage Experiments. The cleavage ability of the complexes was examined following the conversion of pUC18 supercoiled DNA (form I) to nicked circular (form II) and linear DNA (form III) using gel electrophoresis to separate the cleavage products. Three parallel assays were conducted to compare the nuclease activity between complexes **1** and **2**. In all cases, solutions of the copper(II) complexes were freshly prepared by dissolving the crystalline product in the used buffer prior to each experiment. (i) To compare the nuclease activity of the tested complexes, reactions were performed by mixing 6 μL of complex solution (or $CuCl_2$ as a control), 0.5 μL of pUC18 DNA solution (0.5 μg/μL, 1500 μM bp), and 13.5 μL of buffer (50 mM Tris-HCl, pH 7.2), reaching a total volume of 20 μL (final concentrations: 20 μM for **1** and **2**, 40 μM for $CuCl_2$). Then, the samples were incubated at three different temperatures (35, 40, and 50 °C) for 2 h using a thermal cycler. (ii) To compare the nuclease activity in presence of an activating agent, reactions were carried out by mixing 6 μL of complex solution (or $CuCl_2$ as a control), 0.5 μL of pUC18 DNA solution (0.5 μg/μL, 1500 μM bp), 6 μL of MPA (acid mercaptopropionic) at a 0.5-fold concentration relative to the copper concentration, and 7.5 μL of buffer (50 mM Tris-HCl, pH 7.2), reaching a total volume of 20 μL (final concentrations: 20 μM for **1** and **2**, 40 μM for $CuCl_2$). Then, the samples were incubated at three different temperatures (35, 40, and 50 °C) for 2 h using a thermal cycler. (iii) To compare the possible synergy between MQD and copper complexes, reactions were performed by mixing 6 μL of complex solution, 0.5 μL of pUC18 DNA solution (0.5 μg/μL, 1500 μM bp), and 11.5 μL of buffer (50 mM Tris-HCl, pH 7.2). After 5 min, MQD micelles were added to achieve the desired final metal and MQD concentration, reaching a total volume of 20 μL (final concentrations: 20 μM for **1** and **2**). Then, the samples were incubated at several different temperatures (ranging from 20 to 50 °C) for 2 h using a thermal cycler.

Once the reaction time was consumed in experiments i−iii, a quench buffer solution (4 μL) consisting of bromophenole blue (0.25%), xylenecyanole (0.25%), and glycerol (30%) was added. The solution was then subjected to electrophoresis on 0.8% agarose gel in 0.5× TBE buffer (0.045 M Tris, 0.045 M boric acid, and 1 mM EDTA) containing 2 μL/100 mL of a solution of EB (10 mg/mL) at 80 V for 2 h. The bands were photographed on a capturing system (Gelprinter Plus TDI). A correction factor of 1.31 was used for supercoiled DNA because the intercalation between EB and form I DNA is relatively weak compared to that of nicked (form II) and linear (form III) DNA.[81] The fraction of each form of DNA was calculated by dividing the intensity of each band by the total intensities of all bands in the lane.

To test for possible complex−DNA interaction sites, various groove binders were added to the reaction mixtures. The groove binders used were Hoechst 33258 (40 μM) and methyl green (20 μM). Samples were treated as described above in the presence of MPA.

To test for the presence of reactive oxygen species (ROS) generated during strand scission in the presence of QD, various reactive oxygen intermediate scavengers were added to the reaction mixtures. The scavengers used were urea (0.5 mM), *t*-BuOH (4 μL), Tiron (10 mM), 2,2,6,6-tetramethyl-4-piperidone (0.5 mM), and DABCO (0.5 mM). In addition, a chelating agent of copper(I), neocuproine (100 μM), was also assayed. Samples were treated as described above in the presence of MQD.

All of the results are the average of experiments performed at least in triplicate.

AFM measurements were performed in a JPK Nanowizard II AFM and Nanoworld FM cantilevers. The adducts DNA−MQD were prepared by mixing 1 μL of pUC18 DNA (0.25 μg/μL), 2 μL of 600 nM MQD, and 237 μL of buffer (50 mM HEPES, pH 7.0), reaching a total volume of 240 μL. The adducts DNA−MQD−metal complex were prepared by mixing 1 μL of pUC18 DNA (0.25 μg/μL), 2 μL of MQD (600 nM), 4 μL of **1** (0.25 mM), and 233 μL of buffer (50 mM HEPES, pH 7.2), reaching a total volume of 240 μL. The DNA control consisted of 1 μL of pUC18 DNA (0.25 μg/μL) and 239 μL of HEPES buffer, and the MQD control consisted of 2 μL of MQD (600 nM) and 238 μL of HEPES buffer. Then, all of the samples were incubated at 37 °C for 2 h using a thermal cycler.

For sample immobilization, the samples described above were immobilized onto mica by placing 30 μL of the corresponding solution on the surface. Right before its use, the mica was cleaved and functionalized for 30 min with 0.5 μM (3-aminopropyl)triethoxysilane (APTES) to increase sample adsorption. The sample solutions were incubated for 5 min, after which they were carefully rinsed three times with 300 μL of nanopure water without drying. Then, they were left in liquid for another 30 min before removing the water with a pipet and drying the surface in an Ar stream.

For imaging measurements, the samples were imaged in air using a JPK Nanowizard II AFM operating in intermittent contact mode and Nanoworld FM cantilevers at scan rates of 0.5−1 Hz.

XPS experiments were performed in a SPECS Sage HR 100 spectrometer with a nonmonochromatic X-ray sources using a Mg Kα line of 1253.6 eV and an applied power of 250 W calibrated using the $3d_{5/2}$ line of Ag. The selected resolution for the spectra was 15 eV of pass energy and 0.15 eV/step. All measurements were made in an ultra-high-vacuum (UHV) chamber at a pressure of around 5×10^{-8} mbar. The mixture copper complex−MQD was prepared by mixing 100 μL of copper complex (1 mM) and 50 μL of MQD(1 μM), reaching a total volume of 150 μL. The samples were incubated at 37 °C for 2 h using a thermal cycler and were then deposited onto a Si substrate, forming a thin film several monolayers thick. The controls were prepared in the same way.

RESULTS AND DISCUSSION

Crystal Structure of $[Cu_2(\mu\text{-Hdatrz})(phen)_2(H_2O)_2(NO_3)_4]$ (1). X-ray crystallographic data are compiled in Table 1. The lattice of **1** is composed of discrete neutral dinuclear species. The crystal structure of **1** is depicted in Figure 1 together with the numbering scheme (full numbering scheme is given in Figure S1a). Selected bond distances and angles are listed in Table 2.

In the dinuclear unit, two crystallographically independent copper nuclei are linked by one μ-*N*(1),*N*(3)-guanazole ligand (*N*2,*N*4-triazole bridging mode), resulting in a Cu···Cu′ distance of 6.132(3) Å. The guanazole ligand is present in its neutral form. Both copper ions exhibit a tetragonal geometry. Each metal center is chelated by one phen in equatorial coordinating positions; the other two equatorial sites are occupied by the N-triazole atom (with bond distances of 2.005(2) and 2.010(2) Å) and the O atom of a water molecule (at 1.954(2) and 1.967(2) Å). The four axial positions are filled by monodentate nitrate anions at longer (semicoordinating)

dx.doi.org/10.1021/ic4027249 | Inorg. Chem. 2014, 53, 578−593

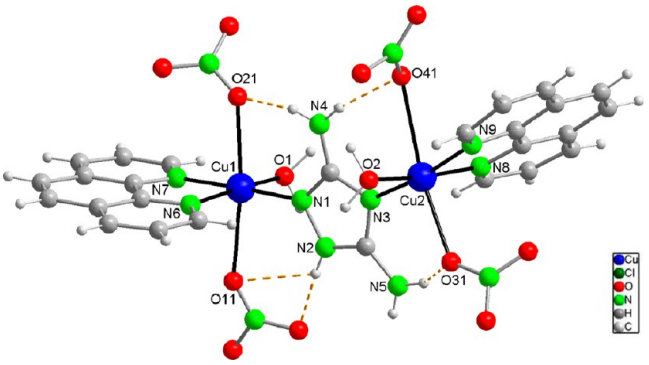

Figure 1. View of the structure of **1** showing the numbering scheme and intramolecular hydrogen bonds.

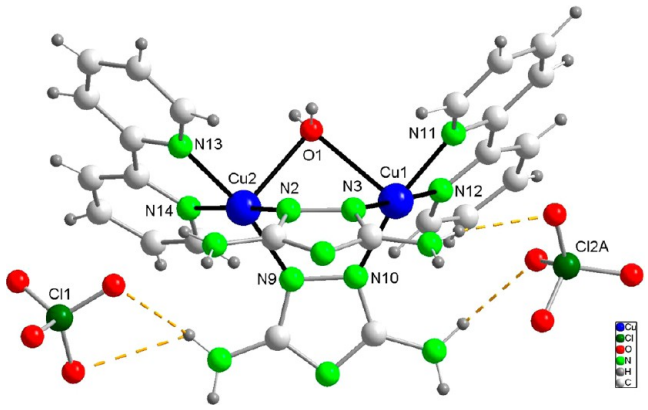

Figure 2. View of the structure of **2** showing the numbering scheme and the hydrogen bonds that attach the perchlorate anions to the dimeric unit.

distances in the 2.404(3)−2.692(3) Å range. Both copper(II) centers can therefore be described by $CuN_3O + O'_2$ coordination. The Cu−N−C bond angles at the triazole bridging region are 136.4(2) and 129.0(2)°. The planes defined by the two phen molecules form a dihedral angle of 40.8(1)°, a value comparable to that reported for the two phen molecules in the structure of $[Cu(phen)_2](ClO_4)_2$ (49.9°).[82,83] In turn, in **1** each phen plane forms a dihedral angle with the central triazole ring of 75.6(1) and 84.2(1)°. Hence, the two ligands of each copper ion are quasi perpendicular (Figure S1b).

In the network of **1**, strong intramolecular (Figure 1) and intermolecular (Figure S2) hydrogen bonds stabilize the dinuclear units (Table S1). Figure S2 exhibits the packing views of compound **1**. The interconnection of dimeric units takes place through hydrogen bonding and stacking interactions between phen fragments, with the shortest ring-to-ring distances being in the range of 3.7−3.9 Å.

Crystal Structure of $[Cu_2(\mu\text{-datrz})_2(\mu\text{-OH}_2)(bipy)_2](ClO_4)_2$ (2). X-ray crystallographic data are listed in Table 1. The lattice of **2** is made up of dinuclear cations and two perchlorate anions per cation. The crystal structure of **2** is depicted in Figure 2 together with the numbering scheme (full numbering scheme is given in Figure S3). Selected bond distances and angles are included in Table 3.

In the dinuclear unit, the two copper centers, which are crystallographically independent, are triply bridged by two μ-*N*1,*N*2-triazolato ligands and one water molecule, leading to a short Cu···Cu′ distance of 3.317(1) Å. The ligand, guanazole, is present in its anionic form (i.e., as guanazolato). Both copper ions exhibit distorted square pyramidal environments, with two triazole N atoms and the two bipy N atoms in equatorial positions, and the bridging O(1) water atom in the apical site, providing $CuN_4 + O'$ coordination. With the bridging system taken into account, compound **2** compares well to the previously reported $[Cu_2(\mu\text{-Hdatrz})_2(\mu\text{-OH}_2)(H_2O)_4(SO_4)](SO_4)\cdot 3.5H_2O$ (**3**) compound.[84] The main differences between **2** and **3** are the presence of the two chelating bipy ligands instead of water molecules on equatorial positions and the anionic character of the guanazole bridge. In **2**, the observed Cu−N(triazole) distances, ranging from 1.949(3) to 1.991(4) Å, are shorther than those usually observed for dinuclear *N*1,*N*2-triazole-bridged Cu(II) compounds and are even slightly shorther than those found in

Table 2. Selected Bond Lengths (Å) and Angles (Degrees) for 1

Cu(1)−O(1)	1.954(2)	Cu(2)−O(2)	1.967(3)
Cu(1)−N(6)	1.994(2)	Cu(2)−N(8)	2.011(3)
Cu(1)−N(7)	2.005(2)	Cu(2)−N(3)	2.010(2)
Cu(1)−N(1)	2.005(2)	Cu(2)−N(9)	2.027(3)
Cu(1)−O(21)	2.422(2)	Cu(2)−O(31)	2.404(3)
Cu(1)−O(11)	2.492(3)	Cu(2)−O(41)	2.692(3)
Cu(1)−Cu(2)	6.132(3)		
O(1)−Cu(1)−N(6)	172.90(9)	O(2)−Cu(2)−N(8)	172.15(10)
O(1)−Cu(1)−N(7)	91.94(10)	O(2)−Cu(2)−N(3)	90.85(11)
N(6)−Cu(1)−N(7)	82.63(9)	N(8)−Cu(2)−N(3)	96.12(9)
O(1)−Cu(1)−N(1)	91.50(11)	O(2)−Cu(2)−N(9)	90.56(11)
N(6)−Cu(1)−N(1)	93.86(10)	N(8)−Cu(2)−N(9)	82.05(10)
N(7)−Cu(1)−N(1)	176.43(9)	N(3)−Cu(2)−N(9)	172.01(9)
O(1)−Cu(1)−O(21)	91.29(11)	O(2)−Cu(2)−O(31)	91.04(14)
N(6)−Cu(1)−O(21)	93.01(9)	N(8)−Cu(2)−O(31)	91.78(12)
N(7)−Cu(1)−O(21)	87.17(8)	N(3)−Cu(2)−O(31)	96.26(9)
N(1)−Cu(1)−O(21)	93.69(9)	N(9)−Cu(2)−O(31)	91.58(9)
O(1)−Cu(1)−O(11)	90.92(15)	O(2)−Cu(2)−O(41)	85.72(10)
N(6)−Cu(1)−O(11)	84.22(13)	N(8)−Cu(2)−O(41)	89.81(8)
N(7)−Cu(1)−O(11)	86.82(10)	N(3)−Cu(2)−O(41)	97.25(8)
N(1)−Cu(1)−O(11)	92.19(11)	N(9)−Cu(2)−O(41)	75.01(8)
O(21)−Cu(1)−O(11)	173.67(9)	O(31)−Cu(2)−O(41)	166.14(8)

dx.doi.org/10.1021/ic4027249 | *Inorg. Chem.* 2014, 53, 578−593

Table 3. Selected Bond Lengths (Å) and Angles (Degrees) for 2

Cu(1)−N(10)	1.948(3)	Cu(2)−N(9)	1.960(3)
Cu(1)−N(3)	1.991(3)	Cu(2)−N(2)	1.979(3)
Cu(1)−N(11)	1.999(3)	Cu(2)−N(14)	2.011(3)
Cu(1)−N(12)	2.007(3)	Cu(2)−N(13)	2.016(3)
Cu(1)−O(1)	2.486(2)	Cu(2)−O(1)	2.356(3)
Cu(1)−Cu(2)	3.3165(6)		
N(10)−Cu(1)−N(3)	88.70(14)	N(9)−Cu(2)−N(14)	94.04(14)
N(10)−Cu(1)−N(11)	167.82(13)	N(2)−Cu(2)−N(14)	173.00(14)
N(3)−Cu(1)−N(11)	97.47(13)	N(9)−Cu(2)−N(13)	168.84(13)
N(10)−Cu(1)−N(12)	93.14(14)	N(2)−Cu(2)−N(13)	95.48(14)
N(3)−Cu(1)−N(12)	178.07(13)	N(14)−Cu(2)−N(13)	80.65(14)
N(11)−Cu(1)−N(12)	80.61(14)	N(9)−Cu(2)−O(1)	98.08(11)
N(10)−Cu(1)−O(1)	96.42(11)	N(2)−Cu(2)−O(1)	88.69(11)
N(3)−Cu(1)−O(1)	87.04(11)	N(14)−Cu(2)−O(1)	97.27(11)
N(11)−Cu(1)−O(1)	94.39(11)	N(13)−Cu(2)−O(1)	92.35(12)
N(12)−Cu(1)−O(1)	93.33(11)	Cu(2)−O(1)−Cu(1)	86.41(8)
N(9)−Cu(2)−N(2)	88.75(13)		

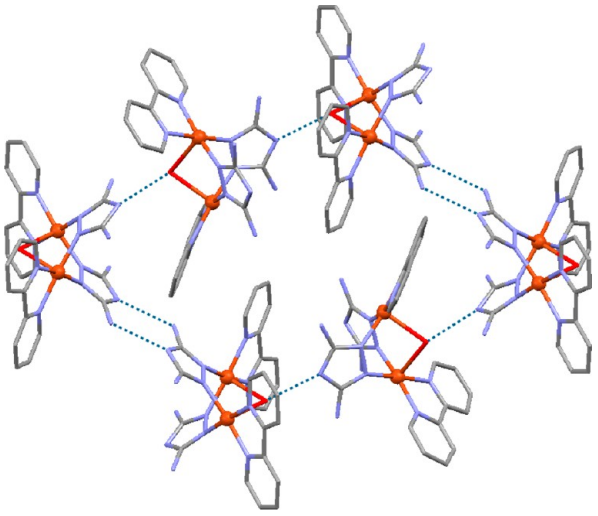

Figure 3. Packing view of complex **2** showing intermolecular hydrogen bonds.

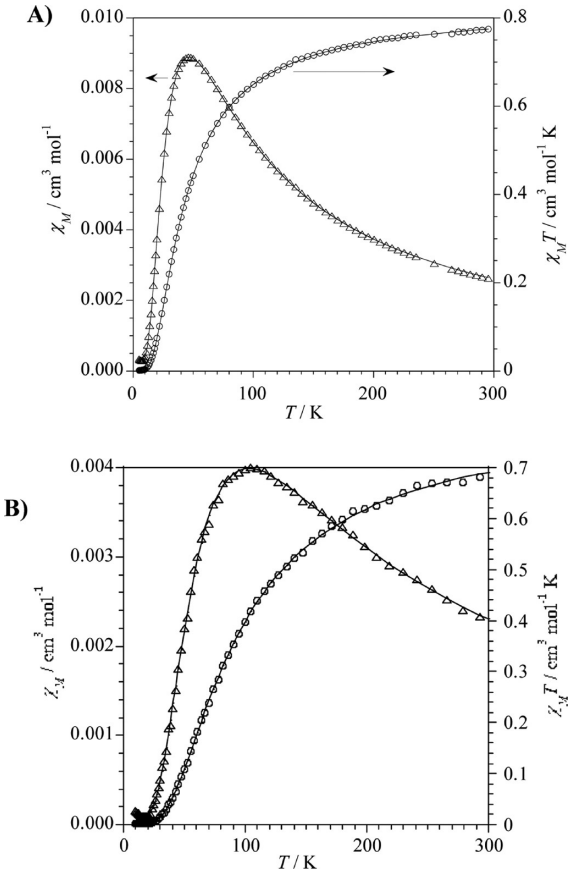

Figure 4. $\chi_M T/\chi_M$ vs T curves for **1** (A) and **2** (B) (χ_M is the magnetic susceptibility per dinuclear unit).

compound **3**.[84−87] This coordination feature must be related to the deprotonation of the guanazole ligand. Cu(1) and Cu(2) are displaced from their corresponding equatorial planes by 0.0924(5) and −0.1400(5) Å, respectively. The two equatorial planes are almost perpendicular; the dihedral angle between them measures 84.7(1)°.

The two Cu−O(1) distances are somewhat different [Cu(1)−O(1) = 2.486(2) Å; Cu(2)−O(1) = 2.356(3) Å]. The angle Cu(1)−O(1)−Cu(2) is 86.41(8)°. The Cu···Cu′ distance [as above indicated, 3.317(1) Å] is significantly shorter than that typical for double-triazole-bridged dicopper(II) compounds [4.085(1)−3.854(6) Å],[88−90] as expected because the μ-OH_2 causes the bridging system to fold, but again, it is slightly shorter than the Cu···Cu′ distance reported for **3** [3.495(1) Å], presumably because of the anionic character of the bridging triazolate. In the bridging system, the Cu−N−N angles of **2**, which range from 118.2(2) to 120.8(2)°, also differ clearly from those of the above-mentioned dimeric Cu(II) structures but are similar to the Cu−N−N angles of compound **3** [119.9(3)−123.3(3)°].

Compound **2** is, together with **3**, one of the few examples of binuclear compounds with two bridging triazole rings and one bridging oxygen atom and consequently with a {Cu−(N−N)$_2$−Cu} framework that is clearly not planar. However, some dicadmium complexes of this type have been reported (i.e., [Cd_2(deatrz)$_2$(H_2O)-Br_4] (deatrz = 3,5-diethyl-4-amino-1,2,4-triazole)).[91]

Figure 3 displays a packing view of the structure. As mentioned, the bridging μ-OH_2 folds the structure. In each dimeric unit, the planes defined by the two bipy molecules form a dihedral angle of 64.0(1)°, and the two datrz planes define a dihedral angle of 73.2(1)°. It can be considered that the structure lacks significant stacking interactions. In contrast,

dx.doi.org/10.1021/ic4027249 | Inorg. Chem. 2014, 53, 578−593

Scheme 2

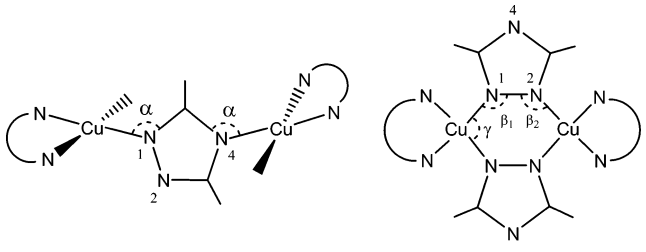

(a) compound **1** (b) compound **2**

there is an important hydrogen-bond network (Table S2). Thus, the dimeric units are connected through the strong intermolecular H-bond established between the bridging μ-OH_2 of one dimeric unit and the N(4) triazole atom of the contiguous unit [d(D···A) = 2.824(4) Å] to give chains. Moreover, the chains are connected through double H-bonds formed between the pairs N(7)···H–N(8)* and N(8)–H···N7* of neighboring guanazolate ligands to provide layers (Figure 3); these are further linked via additional hydrogen bonds that involve the perchlorate anions, thus resulting in a 3D supramolecular network (Figure S4).

Magnetic Properties of 1. The temperature dependences of the $\chi_M T/\chi_M$ values for **1** and **2** are shown in Figure 4 (χ_M is the magnetic susceptibility per two Cu(II) ions). At room temperature, the $\chi_M T$ value agrees well (for **1**) or approximately well (for **2**) with that expected for two noninteracting Cu(II) ions. The χ_M curve increases as the temperature is lowered to reach maxima at ca. 50 K (**1**)/100 K (**2**) and then decreases to lower temperatures. The occurrence of this maximum in χ_M is characteristic of weak-to-moderate antiferromagnetic (AF) coupling between the magnetic ions through the μ-triazole ligand. Below 10 K (**1**)/20 K (**2**), a tail is observed, which is due to the presence of a small amount of paramagnetic impurity. In accordance with the existence of AF coupling leading to an $S = 0$ ground state, the $\chi_M T$ curve exhibits first a slight decrease and then a sharp decrease to ca. 10 K (**1**)/20 K (**2**). The magnetic data of **1** and **2** were fitted to the theoretical equation derived from the isotropic Hamiltonian: $\mathbf{H} = -J\mathbf{S}_1\mathbf{S}_2$. Assuming that the g factors for both Cu(II) ions are identical, the best fit parameters were $J = -52.1$ cm^{-1}, $g = 2.10$ (the percentage of paramagnetic impurity was considered negligible) for **1**, and $J = -115.0$ cm^{-1}, $g = 2.09$, and $\rho = 0.35\%$ for **2**.

The magnetic properties of **1** are clearly of interest owing to the lack of magnetic data for discrete Cu···Cu′ dimers with a *NCN*-triazolyl bridge (*N*2,*N*4-triazole bridging mode). As indicated above, in **1** the copper atoms exhibit a 4 + 2 tetragonally elongated octahedral coordination, with the d_{x2-y2} magnetic orbital directed toward the $N_{triazole}$ and N_{phen} nitrogen atoms (Scheme 2). In a first approach, the superexchange σ pathway should depend on the bond angles at the coordinating N atoms of the triazole bridge (α_1 = Cu$_1$–N$_{trz}$–C$_{trz}$ and α_2 = Cu$_2$–N$_{trz}$–C$_{trz}$).[31] In contrast, with the absence of comparable *NCN*-triazolyl dicopper(II) complexes, the literature contains abundant complexes with *NCN*-imidazolyl[92−101] and a few with *NCN*-tetrazolyl[102] bridges, for which the magnetic exchange parameter, J, has been determined. Attempts at finding magneto-structural correlations have been performed for both types of bridges. For the tetrazole system, Colacio et al. established that a main factor determining the AF coupling is the value of the Cu–N$_{tetraz}$–C$_{tetraz}$ angle (α), that is, the greater the Cu–N–C angle, the stronger is the AF interaction.[102] Plass et al.[92] and more recently García-España et al.,[101] after analyzing the extensive family of the imidazole-bridged compounds, concluded that there is not a simple magneto-structural relationship between geometric parameters and J, given that J depends on the bridging ligand but also on the non-bridging ligands ($-J$ values ranging from 24 to 88 cm^{-1}).[92,101] García-España et al. specifically indicated that, apart from the α angle, several parameters such as Cu–N(Im) bond distances, donor-atoms of the peripheral ligands, and values of the τ distortion parameter (in the case of penta-coordinated copper centers) may influence the magnetic exchange and contribute to the overall interaction. J values and α data for selected closely related complexes (**a**–**e**) have been compiled in Table 4 to give a context for triazole compound **1**. The short list clearly evidences that the Cu–N–C angle alone does not explain the magnitude of the magnetic exchange but suggests that the J value of **1** can be considered as medium among the J values for *NCN* bridges.

In compound **2**, the two Cu(II) ions are linked by three bridges. From the crystal structure, it could be considered that, like in compound **1**, the magnetic exchange occurs via the d_{x2-y2} orbitals on the Cu(II) ions that overlap with the σ orbitals of the N atoms of the triazole bridges, which are placed at equatorial positions. Exchange interaction through the pathway provided by the large axial bonding (through the μ-OH_2) is expected to have little relevance because of the low unpaired electron density along the d_{z2} orbital of the copper atoms. In principle, at least from a magnetic point of view, compound **2** could be compared to related bis(μ-*N*1,*N*2-triazole)-bridged Cu(II) complexes (Scheme 2). However, it should be noted that in most of those complexes the [Cu$_2$L$_2$] unit is planar. As mentioned above, compound **2** is only the second case of a folded dicopper(II) compound of this class, the first one having been reported earlier by us (compound **3**).[84] Table 5 includes the structural parameters involved in the bridging

Table 4. Bridging Angles and Magnetic Exchange Coupling for Selected (Closely Related) Dinuclear *NCN*-Bridged Copper(II) Compounds[a]

compound[b]	α = Cu–N$_{ring}$–C$_{ring}$ (degrees)	$-J$ (cm^{-1})	ref
[Cu$_2$(μ-tetrz)(tren)$_2$](ClO$_4$)$_3$	131, 131	31	102
[Cu$_2$(μ-mim)(dien)$_2$](ClO$_4$)$_3$	132, 133	75	92
[Cu$_2$(μ-im)(dien)$_2$](ClO$_4$)$_3$	125, 126	64	92
[Cu$_2$(μ-bim)(dien)$_2$](ClO$_4$)$_3$	123, 124	37	92
[Cu$_2$(μ-imi)(phen)$_4$](NO$_3$)$_3$	124, 126	24	94
[Cu$_2$(μ-Hdatrz)(phen)$_2$(H$_2$O)(NO$_3$)$_4$] (**1**)	129, 136	52	this work

[a]See Scheme 2. [b]tetrz = tetrazole ligand; tren = tris(2-aminoethyl)amine; mim, im, bim, and imi are imidazole ligands; dien = diethylentriamine; phen = 1,10-phenanthroline; and Hdatrz = 3,5-diamino-1,2,4-triazole = guanazole.

dx.doi.org/10.1021/ic4027249 | Inorg. Chem. 2014, 53, 578−593

Table 5. Magnetic and Structural Parameters for Dinuclear Bis(*N*1,*N*2-triazole)-Bridged Copper(II) Compounds with a Folded $\{Cu-N-N\}_2$ Ring[a]

compound[b]	γ = N−Cu−N (avg) (degrees)	β_1 = $Cu_1-N_1-N_2$ (avg) (degrees)	β_2 = $Cu_2-N_2-N_1$ (avg) (degrees)	Cu···Cu′ (Å)	$-J$ (cm^{-1})	ref
$[Cu_2(\mu\text{-Hdatrz})_2(\mu-OH_2)(H_2O)_4(SO_4)](SO_4)$ (**3**)	92.4	122.2	120.8	3.495	94	84
$[Cu_2(\mu\text{-datrz})_2(\mu-OH_2)(bipy)_2](ClO_4)_2$ (**2**)	88.7	119.9	118.1	3.317	115	this work
$[Cu(\mu\text{-bpt})(CF_3SO_3)(H_2O)]_2$[c]	90.2	134.7	135.0	4.085	236	90

[a]See Scheme 2. [b]Hdatrz = guanazole; bipy = bipyridine; and avg = averaged values. [c]This compound with a planar $\{Cu-N-N\}_2$ ring shows one of the highest J values; it has been included here to provide a set of reference data; bpt = 3,5-bis(pyridin-2-yl)-1,2,4-triazolate.

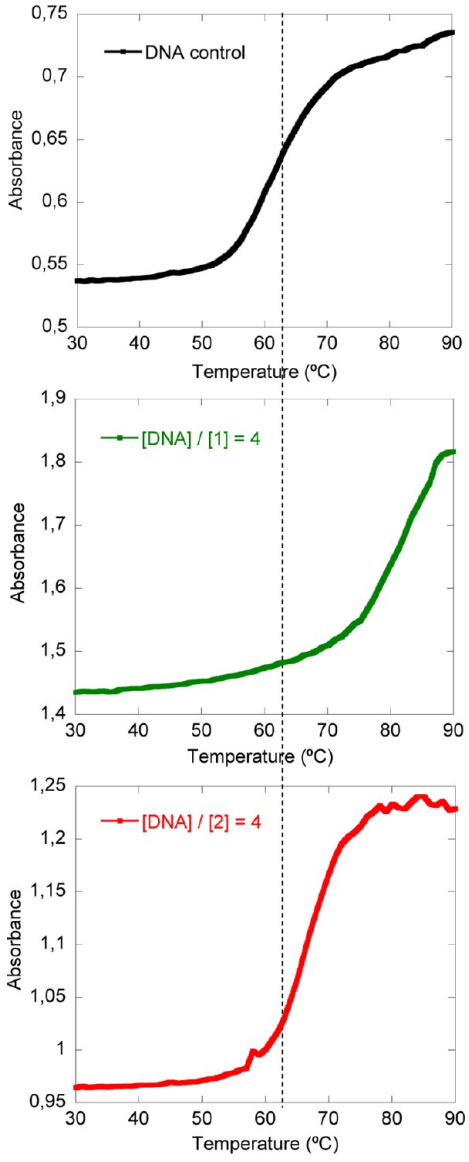

Figure 5. DNA melting-temperature profile of CT-DNA (100 μM): (top) in the absence of complex, (middle) with complex **1** (25 μM), and (bottom) with complex **2** (25 μM).

system and the J values for both complexes. The magnetic coupling of **2**, like that of **3**, is lower than that reported for the analogous symmetric $[Cu_2L_2]$ planar systems,[84,88−90] probably because the folding of the bridging system causes less overlap between the magnetic orbitals of the metal centers and the σ orbital of the ligand. Still, the magnetic exchange of **2** is somehow higher than that of **3**. This fact must be result of the deprotonation

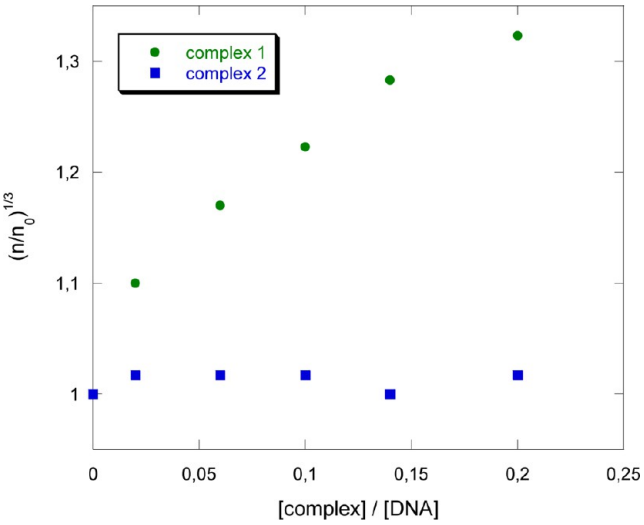

Figure 6. Viscosimetry titration of complexes **1** and **2**.

of the guanazole in **2**, which leads to shorter Cu−N bonding distances and larger magnetic orbitals overlap than in **3**.

DNA-Binding and DNA-Cleavage Properties. The study of the DNA-binding properties was carried out for **1** and **2** through a series of techniques: thermal denaturation, viscosimetry, and fluorescence-based assays. Both complexes were prepared and isolated as solid products (see the Experimental Section) and then dissolved in water for the biological experiments.

The existence of the dinuclear unit of **1** and **2** in solution was tested by mass spectrometry. The electrospray mass spectrum (in positive mode) of complex **1** shows a peak at m/z = 708, corresponding to the species $\{[Cu_2(\mu\text{-Hdatrz})(phen)_2(NO_3)_2]\text{-}H\}^+$, which indicates that the complex is present as dinuclear cation in solution (Figure S5a). Similarly, for compound **2**, a peak at m/z = 652 that can be assigned to the $\{[Cu_2(\mu\text{-datrz})_2(\mu\text{-}H_2O)(bipy)_2]\text{-}H\}^+$ species confirms the existence of this complex in solution (Figure S5b).

DNA Binding Properties. Figure 5 shows the shift in melting temperatures (ΔT_m) resulting from the association of **1** and **2** with CT-DNA. The ΔT_m produced by **1** is high and notably larger than by **2** (20 vs 5 °C), which implies that the stabilization of the DNA double strand produced by **1** is more pronounced. The literature shows that classical intercalators like ethidium bromide (EB) increase the T_m of double-helical DNA moderately (7.2 °C).[79] Additionally, classical groove binders like Hoescht 33258 or distamycin (and related unfused aromatic heterocycles; positively charged) bind electrostatically in the minor groove, thus stabilizing sequences of DNA and raising the T_m greatly (>25 or 21 °C, respectively).[79] Because intercalators but not groove binders cause lengthening,

dx.doi.org/10.1021/ic4027249 | Inorg. Chem. 2014, 53, 578−593

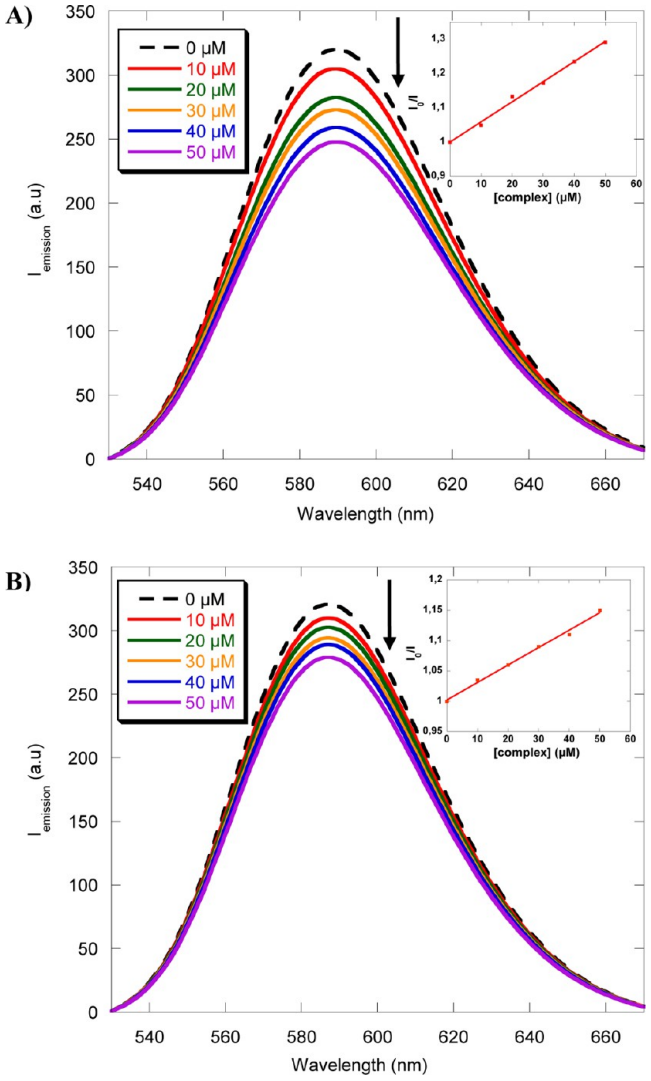

Figure 7. Emission spectra of EB bound to CT-DNA in the absence (dotted line) and presence (continuous line) of (A) complex **1** and (B) complex **2**. The arrow shows the changes in intensity at increasing concentrations of the complex. The inset shows the Stern–Volmer graph ([complex] vs I_0/I_F). [CT-DNA] = [EB] = 50 μM.

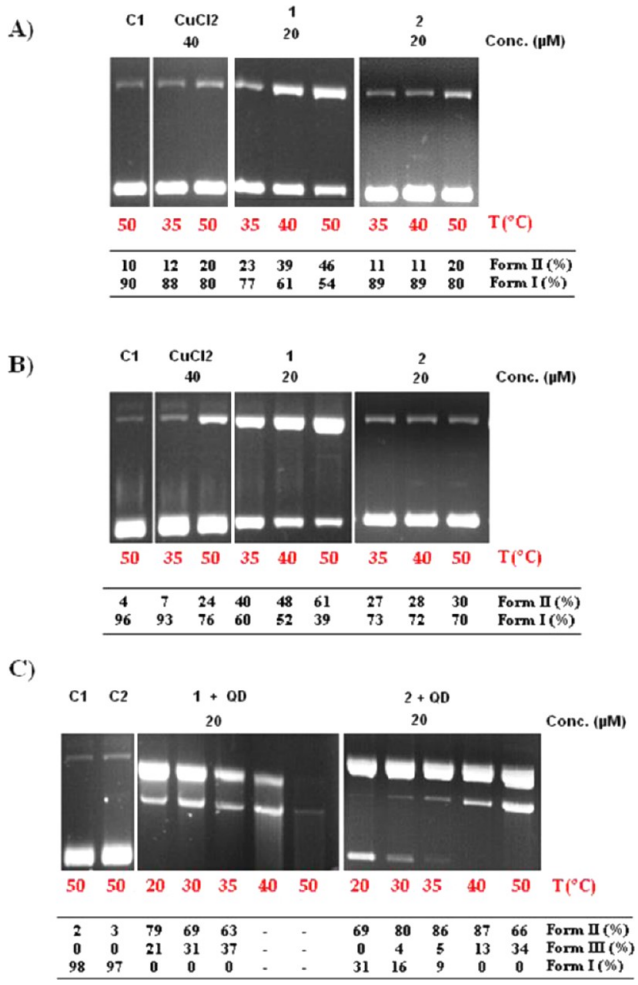

Figure 8. Representative plasmid cleavage assays of supercoiled pUC18 DNA (37.5 μM) promoted by $CuCl_2$ and complexes **1** and **2** at different temperatures in 50 mM Tris HCl buffer, pH 7.2, after 2 h. C1 corresponds to DNA control and C2, DNA + QD (15 nM). (A) Absence of activating agent. (B) Presence of MPA (10 μM). (C) Presence of MQD (15 nM). QD = QD-filled micelles containing a 1:1 mixture of DSPE-PEG(2000) amine and PEG(2000) PE.

stiffening, and unwinding of DNA structure and because viscosity is proportional to L^3 for a rod-like DNA structure of length L,[103,104] we carried out viscosity measurements. Of the two dicopper(II) complexes, only **1** increases the CT-DNA viscosity as the metal complex/DNA ratio is increased (Figure 6). Thus, the viscosity measurements indicate that **1** acts as intercalator, whereas **2** does not. These results taken together suggest that the physical association of **1** with DNA combines intercalation and groove binding through electrostatic and/or hydrogen-bonding interactions.

The binding of **1** and **2** to CT-DNA was also investigated by fluorescence assays by evaluating the fluorescence emission intensity of the EB–DNA system upon addition of the two compounds. In this assay, if a compound is capable of replacing the intercalated EB, then the emission intensity at 595 nm of EB will be reduced.[78−80,105] Indeed, when **1** and **2** were added to a solution of the EB–DNA system (fixed amount) (Figure 7), the two compounds produced a partial removal of EB, yielding linear Stern–Volmer plots fitting the classical equation $I_0/I = 1 + K_{SV}[Q]$. In this equation, I_0 and I are the fluorescence intensities in the absence and presence of the quencher (Q), respectively, and [Q] is the concentration of the quencher, enabling the linear Stern–Volmer quenching constant, K_{SV}, to be determined from the slope. The quenching constants, K_{SV}, obtained were 5.9×10^3 M^{-1} for **1** and 2.9×10^3 M^{-1} for **2**, which confirms that **1** has a higher DNA affinity than **2**.

Besides intercalation, the X-ray crystal structure of **1** suggests that intramolecular hydrogen bonds would be formed between the N–H groups of the μ-guanazole and any atom that binds to the Cu centers, such as the hydrogen-bond-acceptor groups of the DNA grooves and the phosphate backbone. The X-ray structure of **2** also shows that the N–H groups of the μ-guanazoles are available for intermolecular hydrogen-bonding interactions. Such intra- and intermolecular hydrogen-bonding interactions combined with the positively charged nature of the two compounds could explain the aforementioned DNA-binding results.

DNA-Cleavage Activity. The nuclease activity of complexes **1** and **2** was investigated by agarose gel electrophoresis. The DNA cleavage was monitored by transformation of supercoiled

dx.doi.org/10.1021/ic4027249 | *Inorg. Chem.* 2014, 53, 578−593

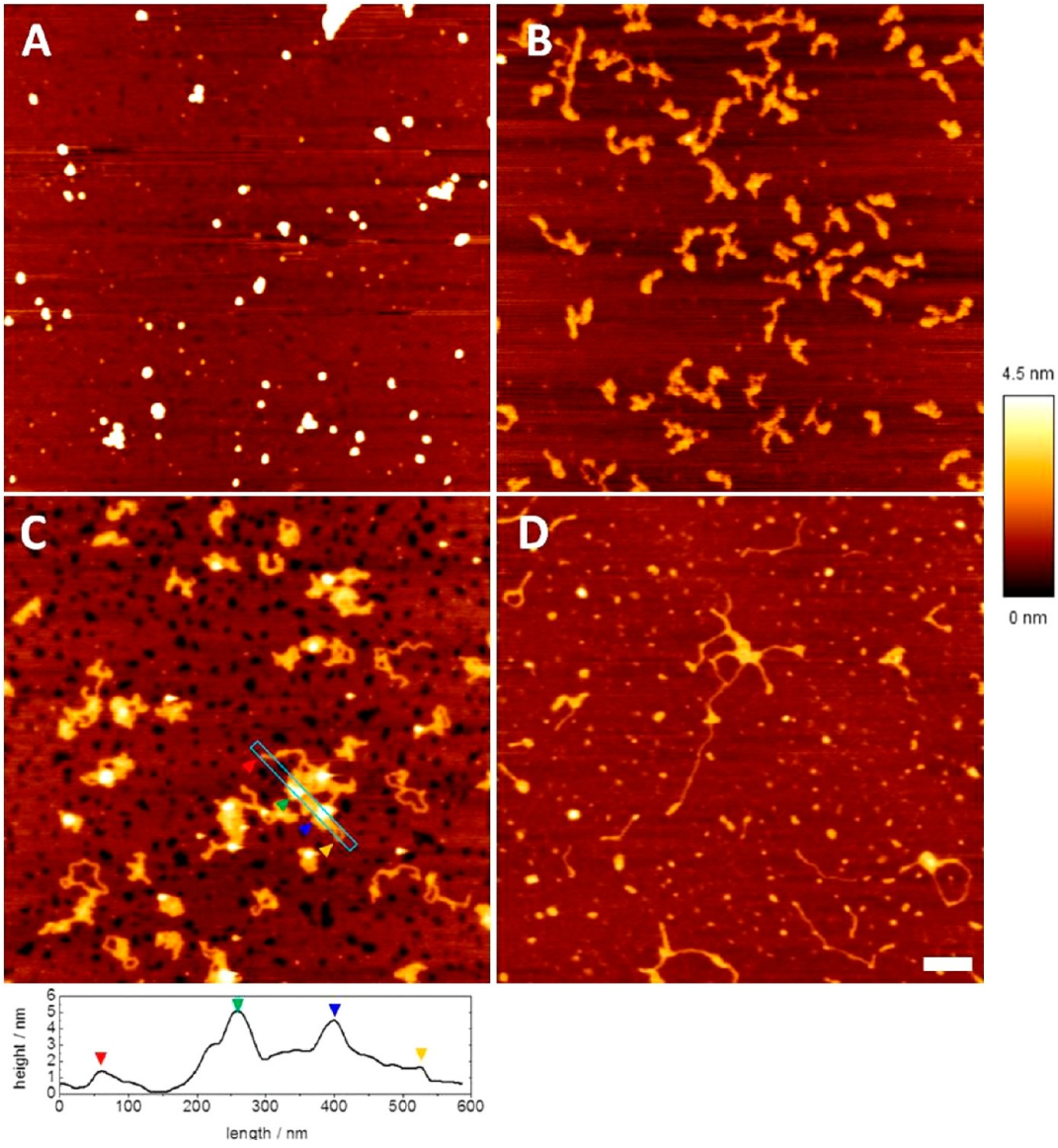

Figure 9. AFM images corresponding to (A) MQD, (B) pUC18, (C) pUC18 + MQD (height profile included), and (D) pUC18 + MQD + **1**.

circular pUC18 DNA (form I) into nicked circular (form II) and linear (form III) forms. The activity was first investigated in the absence and presence of a classical activating agent, 3-mercaptopropionic acid (MPA).

Although compound **2** produces negligible cleavage in the absence of activating agent even at 50 °C, the activity of **1** increases substantially as the temperature is raised from 35 to 50 °C (Figure 8A), suggesting that like other copper(II) complexes this complex may be capable of cleaving DNA by a hydrolytic mechanism.[106−111] In the presence of MPA as reductant (10 μM) (Figure 8B), however, DNA cleavage with **1** increases even further by an oxidative mechanism. This nucleolytic activity with MPA activation is also temperature-dependent. In contrast, compound **2** does not appreciably damage pUC18 either with MPA or with H_2O_2 in the whole range of temperatures.

The possibility of activating compounds **1** and **2** for DNA cleavage by adding water-soluble QD-filled micelles (MQDs) was investigated next. The MQDs were prepared by a self-assembly process of PEGylated phospholipids around hydrophobic CdSe-ZnS core−shell QDs (Scheme 3).[71] Transmission electron microscope (TEM) images and dynamic light scattering (DLS) measurements revealed that the MQDs contained closely packed QDs and a hydrodynamic size of ca. 40 nm (Figure S6).

Fluorescence studies are consistent with binding of the QDMs to DNA. Figure S7 shows a representative assay where the DNA quenches the emission of the MQD solution, which is a sign of adduct formation between the biopolymer and the colloid.[18]

We then imaged the complexes formed between the MQDs and DNA by atomic force microscopy (AFM). In isolation, the MQDs appear as rather homogeneous particles of 36 ± 8 nm in length and 5 ± 2.1 nm in height, features consistent with the hydrodynamic size measurements carried out by DLS (Figure 9). Imaging of plasmid DNA shows a supercoiled structure, in agreement with the agarose gel electrophoresis data (vide infra). Like in other studies, the measured height (0.9 ± 0.2 nm) is lower than the theoretical value of 2 nm, which is mainly due to elastic deformation induced by tip−sample interaction.[112−114] Imaging samples of the plasmid DNA after addition of MQDs clearly shows the binding of the MQDs. Analysis of the cross section of

dx.doi.org/10.1021/ic4027249 | Inorg. Chem. 2014, 53, 578−593

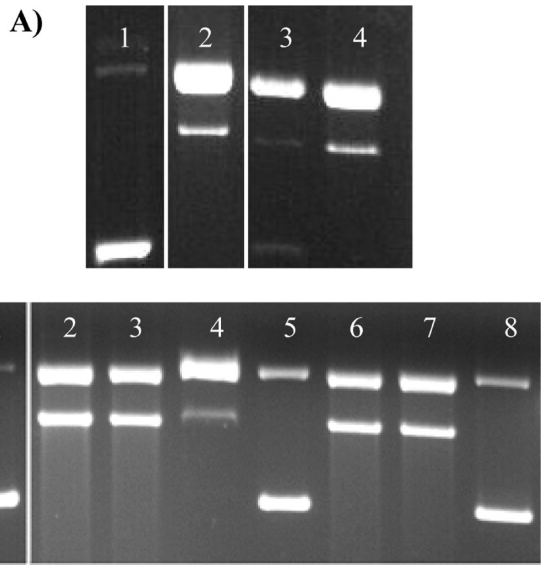

Figure 10. Effect of ROS scavengers or groove binders on the cleavage of supercoiled DNA. (A) Lane 1, DNA control; lane 2, 20 μM complex **1** (+10 μM MPA); lanes 3 and 4, 20 μM complex **1** (+10 μM MPA) plus added agent (lane 3, Hoechst 33258; lane 4, methyl green). (B) Lane 1, DNA control; lane 2, 20 μM complex **1** (+ 15 nM QD); lanes 3–8, 20 μM complex **1** (+ 15 nM QD) plus added agent (lane 3, urea; lane 4, *t*-BuOH; lane 5, Tiron; lane 6, 2,2,6,6-tetramethyl-4-piperidone; lane 7, DABCO; and lane 8, neocuproine). [pUC18 DNA] = 37.5 μM in Tris HCl buffer (pH 7.2), incubation time = 2 h, and T = 35 °C.

the MQD–DNA complex suggests that the DNA wraps around the MQD and provides new experimental evidence to the previous suggestions that QDs can act as protein-like structures. We note that in nature DNA wraps around protein assemblies similar in size to the MQD to form chromatin.[115] To investigate the effect of adding copper complexes to the DNA–MQD complexes, we imaged them after a 2 h incubation. The ability of the copper complexes to cut DNA in the DNA–MQD complexes is clearly detected by the presence of many digested DNA fragments, which in this case, presumably because of their smaller sizes, are not bound to the MQDs.

The gel electrophoresis studies show that compound **1** is strongly activated by the MQDs (Figure 8C). Thus, combined with an extremely small amount of QD (15 nM), compound **1** (20 μM) is capable of generating linear DNA at temperatures as low as 20 °C. Moreover, the linear DNA is gradually degraded into fragments of progressively smaller sizes that appear as smears at physiologically relevant temperatures on the agarose gel. Notably, compound **2**, which was not activated by MPA (10 μM) even at high temperatures, behaves also as an efficient nuclease in the presence of such small quantities of QD. Under these conditions, the MQDs do not cause significant DNA damage; instead, at high QD concentrations, migration of the DNA into the gel is not observed, confirming that MQD–DNA complexes are formed. These results imply that adding MQDs is quite an efficient new strategy for enhancing DNA cleavage of the copper nucleases.

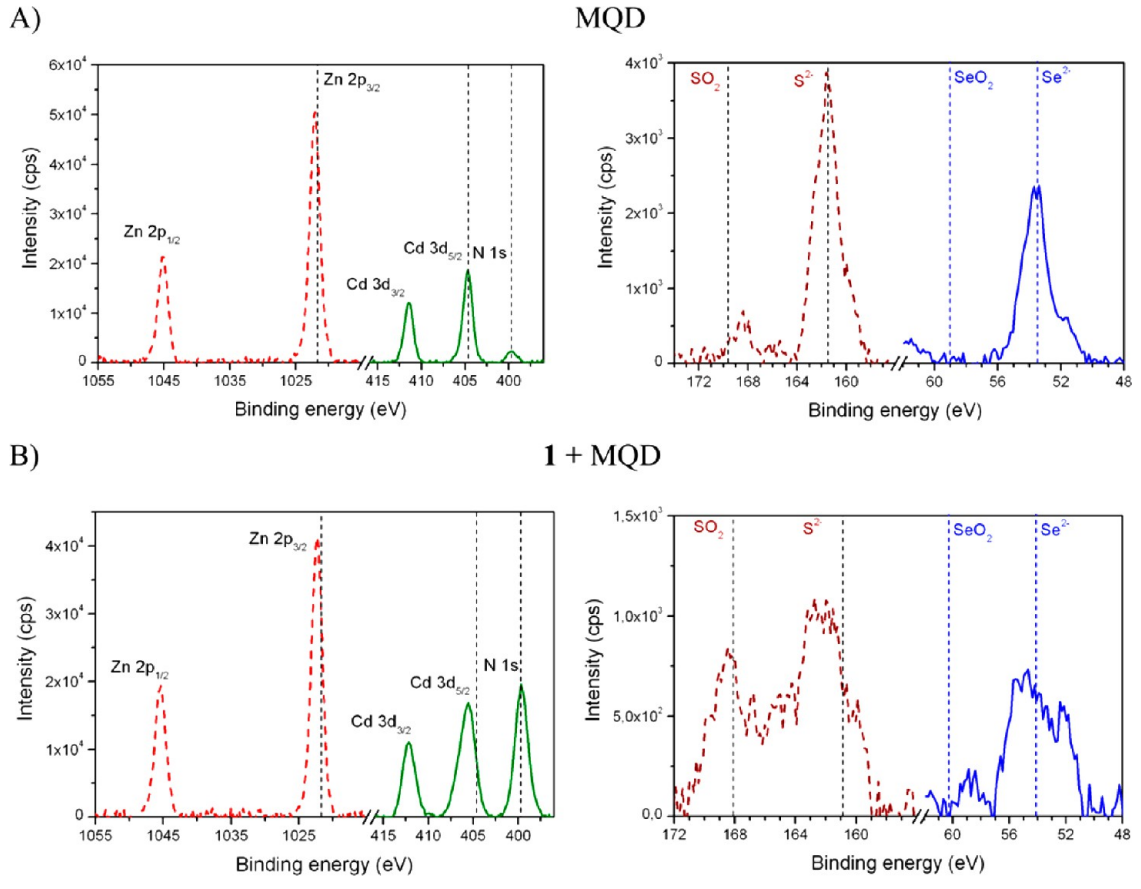

Figure 11. XPS spectra showing the Zn 2p, Cd 3d, S 2p, and Se 3d regions of MQD (A) and **1** + MQD (B) after a 2 h incubation at 37 °C.

dx.doi.org/10.1021/ic4027249 | *Inorg. Chem.* 2014, 53, 578–593

Scheme 3

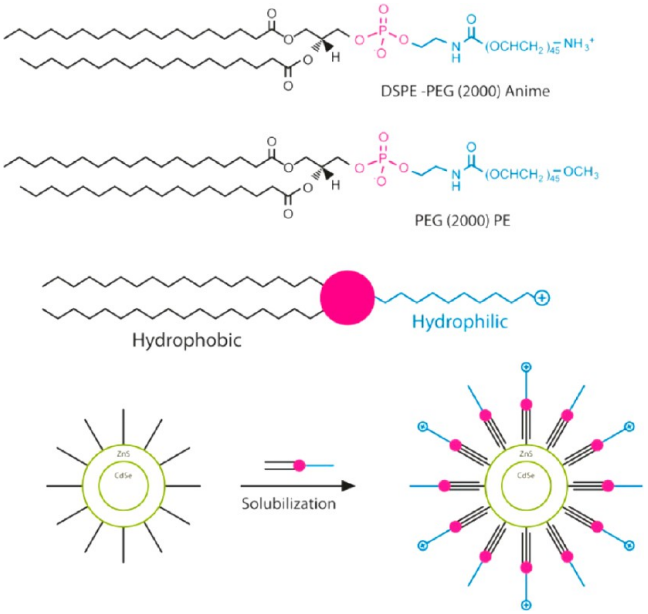

To gain insight into the role of the QD toward enhancing the DNA damage caused by these copper complexes, an analogous micellar system was prepared that was filled with superparamagnetic Fe_3O_4 NPs instead of QDs. The corresponding electrophoresis study shows that, in this case, addition of the magnetic micelles does not lead to enhanced DNA damage by **1** and **2** (Figure S8).

Mechanism of DNA Cleavage and Role of the QDs. To clarify the mechanism (i.e., oxidative vs hydrolytic) of the nuclease activity of complexes **1** and **2**, electrophoresis assays with ROS scavengers (urea and *t*-BuOH for hydroxyl radicals, Tiron for superoxide radicals, and 2,2,6,6-tetramethyl-4-piperidone (TEMP) and diazabicyclo-[2,2,2]-octane (DABCO) for singlet oxygen), groove binders (Hoescht 33258 for minor groove and methyl green for major groove), and a Cu(I)-chelator (neocuproine) were undertaken. In the presence of MPA, inhibition of DNA cleavage is observed for **1** on addition of the minor groove binder Hoescht 33258 (Figure 10A), but the degree of inhibition is relatively low. No inhibition was observed with the major groove binder methyl green in any case. These findings signal the minor groove of the DNA as the nuclease binding site, but in compound **1**, this specificity is lower than, for instance, in $[Cu(phen)_2]^{2+}$, presumably because **1** can interact through electrostatic interactions and hydrogen bonding when the minor groove is inaccessible (vide supra). In the presence of MQDs (Figure 10B), a clear inhibitory effect was found for the superoxide scavenger Tiron, which indicates that the DNA damage produced under these conditions occurs by an oxidative mechanism. Moreover, neocuproine inhibited the DNA degradation, thus pointing to Cu(I) as the intermediate in the oxidative DNA-cleavage reaction.

To identify further the chemical processes involved in the QD-mediated DNA-cleavage process, we carried out X-ray photoelectron spectroscopy (XPS) studies. XPS spectra of MQDs samples taken before and after addition of **1** and **2** under the conditions used for the DNA-cleavage studies show changes in the QD composition. For these MQDs, we detect two strong peaks located at 404.8 and 411.5 eV, corresponding to the Cd 3d binding energy of CdSe and a peak at 53

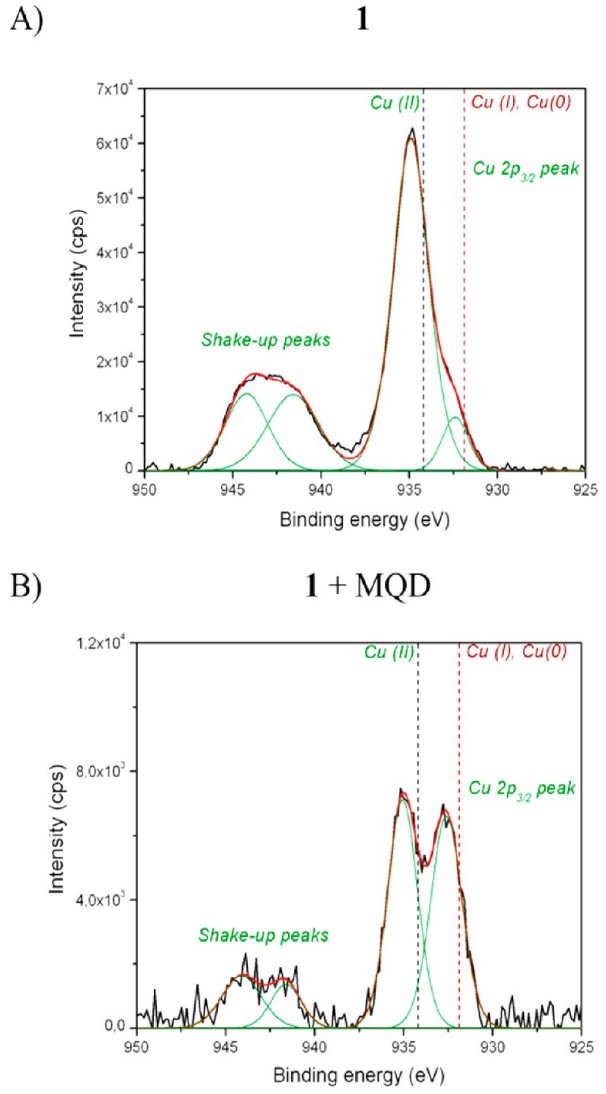

Figure 12. XPS spectrum showing the Cu 2p region of **1** (A) and **1** + MQDs (B) after a 2 h incubation at 37 °C.

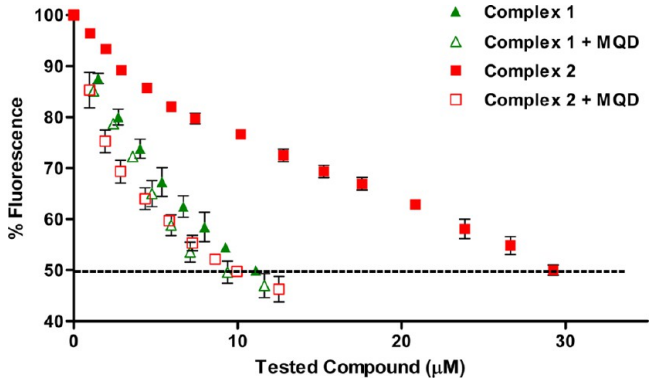

Figure 13. Effect of the addition of **1** and **2** on the emission of CT-DNA bound to EB in the absence and presence of MQDs. [CT-DNA] = 3 μM, [EB] = 3.78 μM, and [QD] = 30 nM.

(6 eV corresponding to the Se 3d transition) (Figure 11). These values match well those reported for other CdSe QDs.[116] The typical peaks for ZnS, with Zn $2p_{3/2}$ and S $2p_{3/2}$ located at 1021.6 and 161.3 eV, respectively, were also observed. However, changes in the S region reveal an oxidation process

dx.doi.org/10.1021/ic4027249 | *Inorg. Chem.* 2014, 53, 578−593

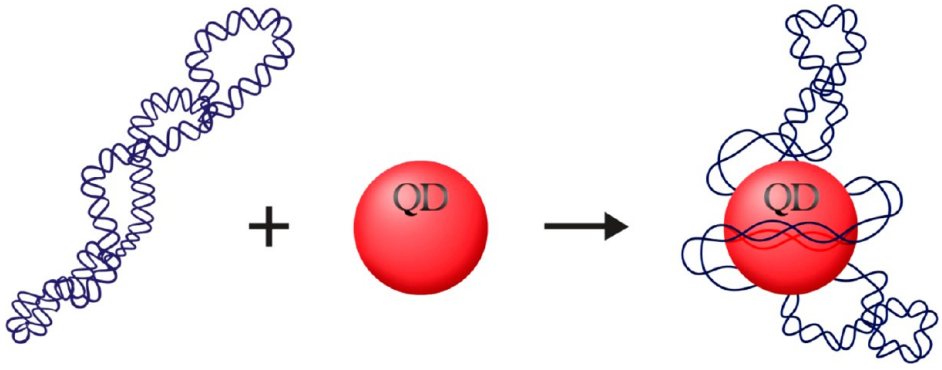

Figure 14. Proposed QD−DNA interaction mode.

after addition of **1** and **2**. The oxidation of the MQDs leads to the appearance of a peak at higher energies than the main S peak because of sulfur dioxide (Figure 11B). Concurrently, we detect reduction of Cu(II) to Cu(I) upon addition of the MQDs. Figure 12 shows the Cu $2p_{3/2}$ spectrum of **1** before and after addition of the MQDs. In addition to a peak at 934.3 eV and the corresponding shakeup satellites characteristic of Cu(II) species, there is a small peak located at 931.9 eV, which can be assigned to Cu(I) species under the acquisition conditions. However, under identical conditions, addition of MQD causes the intensity of the Cu(I) peak to increase significantly. This result is consistent with the inhibition studies and the thermodynamically allowed reduction of Cu(II) to Cu(I) by QDs previously shown by Isarov et al.[117] and more recently by Chan et al.,[118] where electrons are transferred from anionic surface vacancies and/or S on the QD surface to the Cu(II) centers. Adopting the method of Nie et al.,[119] we estimate that the QDs used in this study have 700 S atoms, which could explain the low QD/metal complex ratio (ca. 1:1000) required to activate these copper complexes for DNA cleavage.

In addition to generating the Cu(I) intermediates, we reasoned that forming DNA−MQD complexes could also contribute to the metallonuclease activation process by producing a change in the conformation of DNA that increases the binding sites offered to the nucleases or makes them more susceptible to attack. In this way, the MQD may also promote binding of the metallonuclease to the target DNA. To test this hypothesis, we investigated the ability of **1** and **2** to displace EB from the EB−DNA system before and after the addition of MQDs (Figure 13). By comparing the concentration of the complex needed for a 50% quenching (C_{50}) of the solution containing the EB−DNA system, it is clear that the effect of MQD toward promoting DNA binding is particularly pronounced for **2** (C_{50} = 9.5 and 29 μM in the presence and absence of MQD, respectively). Interestingly, **2** is the complex that interacts less well with DNA (it has lower affinity for DNA than **1** and it does not intercalate) and is completely inactive without mediation of QDs (MPA could not activate **2**).

In summary, by combining three different functional elements, namely, bimetallic complexes, ligands with available hydrogen-bond donors, and QDs, the interaction and cleavage of DNA using **1** and **2** is strongly promoted. The QD participates in the generation of the catalytically active species by acting as a reducing agent that promotes the formation of Cu(I) intermediates. However, compared to external activators such as MPA and H_2O_2, which are needed in micromolar concentrations and only contribute toward the generation of ROS, QDs appear to be much more efficient and versatile, requiring nanomolar concentrations. QDs through their curved surfaces and organic ligands and surface atoms can combine electrostatic interactions, hydrogen bonding, van der Waals and hydrophobic interactions, and release of counterions and solvent from the DNA to promote the formation of QD−DNA complexes. In these QD−DNA complexes, like in DNA−protein complexes, DNA can change its conformation, increasing the binding sites offered to the artificial metallonuclease and/or making them more accessible to the catalytically active species (Figure 14).

CONCLUSIONS

Two novel ternary dicopper complexes with guanazole/ate bridges have been synthesized and characterized. Compound **1** represents the first example of a genuine *N*2,*N*4-triazole-dicopper complex. This has offered the possibility of calculating the magnetic exchange parameter, J($\mu_{2,4}$-triazole) = −52 cm^{-1}, for a couple of Cu(II) centers antiferromagnetically linked through an *NCN*-triazolyl bridge in a discrete molecule. Compound **2**, with a folded [Cu−($N1$−$N2$)$_2$−Cu] bridging system exhibit a higher antiferromagnetic coupling, J ($\mu_{1,2}$-triazolate) = −115 cm^{-1}.

DNA binding and cleavage studies reveal that both compounds can be used as efficient nucleases because of the cooperative effect of the two Cu(II) centers and the guanazole ligand, which in addition to providing a bridge between the two metals can participate in hydrogen-bonding interactions. Of the two complexes, **1** shows the highest affinity for DNA and binds via intercalation of the phen ligands. In the presence of oxygen and micromolar concentrations of MPA or H_2O_2 as activators, only **1** is capable of causing DNA cleavage. However, in the presence of nanomolar concentrations of water-soluble QD-filled micelles, both systems are highly efficient at cleaving DNA.

Overall, we have developed two systems in which different strategies and classes of compounds are successfully combined to yield efficient DNA cleavage by an oxidative mechanism: (1) a bimetallic framework, (2) hydrogen-bonding features and (3) a redox-active protein-like curved nanostructure (QDs). In the case of the most active system, which uses **1** as nuclease, planar aromatic rings capable of DNA intercalation (phen) are also present. The results suggest that their are multiple roles of the QDs toward promoting DNA cleavage by these copper metallonucleases and they combine structural effects with the ability to participate in the generation of intermediates and catalytically active species, which affect DNA cleavage (reactive oxygen species). This new bionanotechnology strategy to enhance the activity of coordination complexes for DNA cleavage is simple and potentially extendable to other redox-active metal complexes. Given the wide range of recognition

dx.doi.org/10.1021/ic4027249 | *Inorg. Chem.* 2014, 53, 578−593

elements that can potentially be incorporated in these MQDs, we anticipate that in the future this novel approach for effecting DNA cleavage will be adopted to impart selectivity; such systems would be extremely attractive for applications in genetic engineering and gene therapy.

■ ASSOCIATED CONTENT

Supporting Information

Selected hydrogen bonds for **1** and **2**, ORTEP views of **1** and **2** showing the full labeling scheme, packing views for **1** and **2**, ESI spectra for **1** and **2**, transmission electron micrograph (TEM) and hydrodynamic size distributions measured by DLS imaging of the MQDs, emission spectra of MQD in the absence and presence of CT-DNA, and plasmid cleavage assays of supercoiled pUC18 DNA promoted by complexes **1** and **2** at 37 °C in the presence of SPIONs. This material is available free of charge via the Internet at http://pubs.acs.org.

■ AUTHOR INFORMATION

Corresponding Authors

*E-mail: sacramento.ferrer@uv.es (S.F.).
*E-mail: jmareque@cicbiomagune.es (J.C.M.-R.).

Present Address

○Cooperative Centre for Research in Biomaterials (CIC biomaGUNE), 20009 San Sebastián, Spain.

Notes

The authors declare no competing financial interest.

■ ACKNOWLEDGMENTS

This work was supported by the Ministerio de Educación y Ciencia (MEC, Spain) (project CTQ2007-63690/BQU) and by the Ministerio de Ciencia e Innovación and FEDER-EC (project MAT2010-15594). J.C.M.-R. acknowledges support by the Ministerio de Economia y Competitividad (MINECO, Spain) (grants CTQ2011-22723 and PRI-PIBIN-2011-0812), the Department of Industry of the Basque Country (grant ETORTEK), and the Department of Education, Universities and Research of the Basque Country (grant PI-2012-33). J.H.G. acknowledges a Ph.D. studenship from the MEC (project CTQ2007-63690/BQU, MEC, Spain). We acknowledge Drs. M. Sales and J. Calvo for ESI-MS assistance, L. Yate for the XPS studies, and A. Cambres-Martínez for graphical work.

■ REFERENCES

(1) Frey, N. A.; Peng, S.; Cheng, K.; Sun, S. *Chem. Soc. Rev.* **2009**, *38*, 2532−2542.
(2) Reiss, P.; Protière, M.; Li, L. *Small* **2009**, *5*, 154−168.
(3) Wang, H.-Q.; Nann, T. *ACS Nano* **2009**, *3*, 3804−3808.
(4) Arvizo, R. R.; Bhattacharyya, S.; Kudgus, R. A.; Giri, K.; Bhattacharya, R.; Mukherjee, P. *Chem. Soc. Rev.* **2012**, *41*, 2943−2970.
(5) Kim, T.-H.; Cho, K.-S.; Lee, E. K.; Lee, S. J.; Chae, J.; Kim, J. W.; Kim, D. H.; Kwon, J.-Y.; Amaratunga, G.; Lee, S. Y.; Choi, B. L.; Kuk, Y.; Kim, J. M.; Kim, K. *Nat. Photonics* **2011**, *5*, 176−182.
(6) Loss, D.; DiVincenzo, D. P. *Phys. Rev. A* **1998**, *57*, 120−126.
(7) Semonin, O. E.; Luther, J. M.; Beard, M. C. *Mater. Today* **2012**, *15*, 508−515.
(8) Sargent, E. H. *Nat. Photonics* **2012**, *6*, 133−135.
(9) Wood, V.; Bulović, V. *Nano Rev.* **2010**, *1*, 5202-1−5202-7.
(10) Liu, Y.; Tolentino, J.; Gibbs, M.; Ihly, R.; Perkins, C. L.; Liu, Y.; Crawford, N.; Hemminger, J. C.; Law, M. *Nano Lett.* **2013**, *13*, 1578−1587.
(11) Resch-Genger, U.; Grabolle, M.; Cavaliere-Jaricot, S.; Nitschke, R.; Nann, T. *Nat. Methods* **2008**, *5*, 763−775.
(12) Medintz, I. L.; Uyeda, H. T.; Goldman, E. R.; Mattoussi, H. *Nat. Mater.* **2005**, *4*, 435−446.
(13) Zhu, H.; Song, N.; Rodríguez-Córdoba, W.; Lian, T. *J. Am. Chem. Soc.* **2012**, *134*, 4250−4257.
(14) Huang, J.; Mulfort, K. L.; Du, P.; Chen, L. X. *J. Am. Chem. Soc.* **2012**, *134*, 16472−16475.
(15) Lakowicz, J. R.; Gryczynski, I.; Gryczynski, Z.; Nowaczyk, K.; Murphy, C. J. *Anal. Biochem.* **2000**, *280*, 128−136.
(16) Hanaki, K.; Momo, A.; Oku, T.; Komoto, A.; Maenosono, S.; Yamaguchi, Y.; Yamamoto, K. *Biochem. Biophys. Res. Commun.* **2003**, *302*, 496−501.
(17) Kotov, N. A. *Science* **2010**, *330*, 188−189.
(18) Mahtab, R.; Harden, H. H.; Murphy, C. J. *J. Am. Chem. Soc.* **2000**, *122*, 14−17.
(19) Mahtab, R.; Rogers, J. P.; Singleton, C. P.; Murphy, C. J. *J. Am. Chem. Soc.* **1996**, *118*, 7028−7032.
(20) Mahtab, R.; Rogers, J. P.; Murphy, C. J. *J. Am. Chem. Soc.* **1995**, *117*, 9099−9100.
(21) Ren, B.; Robert, F.; Wyrick, J. J.; Aparicio, O.; Jennings, E. G.; Simon, I.; Zeitlinger, J.; Schreiber, J.; Hannett, N.; Kanin, E.; Volkert, T. L.; Wilson, C. J.; Bell, S. P.; Young, R. A. *Science* **2000**, *290*, 2306−2309.
(22) Green, M.; Howman, E. *Chem. Commun.* **2005**, 121−123.
(23) Anas, A.; Akita, H.; Harashima, H.; Itoh, T.; Ishikawa, M.; Biju, V. *J. Phys. Chem. B* **2008**, *112*, 10005−10011.
(24) Liang, J.; He, Z.; Zhang, S.; Huang, S.; Ai, X.; Yang, H.; Han, H. *Talanta* **2007**, *71*, 1675−1678.
(25) Hoshino, A.; Fujioka, K.; Oku, T.; Suga, M.; Sasaki, Y. F.; Ohta, T.; Yasuhara, M.; Suzuki, K.; Yamamoto, K. *Nano Lett.* **2004**, *4*, 2163−2169.
(26) Derfus, A. M.; Chan, W. C. W.; Bhatia, S. N. *Nano Lett.* **2004**, *4*, 11−18.
(27) Sykora, M.; Petruska, M. A.; Alstrum-Acevedo, J.; Bezel, I.; Meyer, T. J.; Klimov, V. I. *J. Am. Chem. Soc.* **2006**, *128*, 9984−9985.
(28) Tseng, H.-W.; Wilker, M. B.; Damrauer, N. H.; Dukovic, G. *J. Am. Chem. Soc.* **2013**, *135*, 3383−3386.
(29) Lee, H. J.; Chang, D. W.; Park, S.-M.; Zakeeruddin, S. M.; Grätzel, M.; Nazeeruddin, M. K. *Chem. Commun.* **2010**, *46*, 8788−8790.
(30) Sandros, M. G.; Gao, D.; Benson, D. E. *J. Am. Chem. Soc.* **2005**, *127*, 12198−12199.
(31) Maldonado, C. R.; Touceda-Varela, A.; Jones, A. C.; Mareque-Rivas, J. C. *Chem. Commun.* **2011**, *47*, 11700−11702.
(32) Touceda-Varela, A.; Stevenson, E. I.; Galve-Gasión, J. A.; Dryden, D. T. F.; Mareque-Rivas, J. C. *Chem. Commun.* **2008**, 1998−2000.
(33) Gupta, M.; Caniard, A.; Touceda-Varela, A.; Campopiano, D. J.; Mareque-Rivas, J. C. *Bioconjugate Chem.* **2008**, *19*, 1964−1967.
(34) Stewart, M. H.; Huston, A. L.; Scott, A. M.; Efros, A. L.; Melinger, J. S.; Gemmill, K. B.; Trammell, S. A.; Blanco-Canosa, J. B.; Dawson, P. E.; Medintz, I. L. *ACS Nano* **2012**, *6*, 5330−5347.
(35) Maldonado, C. R.; Salassa, L.; Gomez-Blanco, N.; Mareque-Rivas, J. C. *Coord. Chem. Rev.* **2013**, *257*, 2668−2688.
(36) Chen, K.; Li, Z.-B.; Wang, H.; Cai, W.; Chen, X. *Eur. J. Nucl. Med. Mol. Imaging* **2008**, *35*, 2235−2244.
(37) Maldonado, C. R.; Gómez-Blanco, N.; Jauregui-Osoro, M.; Brunton, V. G.; Yate, L.; Mareque-Rivas, J. C. *Chem. Commun.* **2013**, *49*, 3985−3987.
(38) Burks, P. T.; Ostrowski, A. D.; Mikhailovsky, A. A.; Chan, E. M.; Wagenknecht, P. S.; Ford, P. C. *J. Am. Chem. Soc.* **2012**, *134*, 13266−13275.
(39) Neuman, D.; Ostrowski, A. D.; Mikhailovsky, A. A.; Absalonson, R. O.; Strouse, G. F.; Ford, P. C. *J. Am. Chem. Soc.* **2008**, *130*, 168−175.
(40) Neuman, D.; Ostrowski, A. D.; Absalonson, R. O.; Strouse, G. F.; Ford, P. C. *J. Am. Chem. Soc.* **2007**, *129*, 4146−4147.
(41) Jiang, Q.; Xiao, N.; Shi, P.; Zhu, Y.; Guo, Z. *Coord. Chem. Rev.* **2007**, *251*, 1951−1972.

(42) Mancin, F.; Scrimin, P.; Tecilla, P. *Chem. Commun.* **2012**, *48*, 5545−59.
(43) Sigman, D. S.; Bruice, T. W.; Mazumder, A.; Sutton, C. L. *Acc. Chem. Res.* **1993**, *26*, 98−104.
(44) Chen, C. B.; Milne, L.; Landgraf, R.; Perrin, D. M.; Sigman, D. S. *ChemBioChem* **2001**, *2*, 735−740.
(45) Spassky, A.; Sigman, D. S. *Biochemistry* **1985**, *24*, 8050−8056.
(46) Kuwabara, M.; Yoon, C.; Goyne, T.; Thederahn, T.; Sigman, D. S. *Biochemistry* **1986**, *25*, 7401−7408.
(47) Perrin, D. M.; Chen, C.-h. B.; Xu, Y.; Pearson, L.; Sigman, D. S. *J. Am. Chem. Soc.* **1997**, *119*, 5746−5747.
(48) Milne, L.; Xu, Y.; Perrin, D. M.; Sigman, D. S. *Proc. Natl. Acad. Sci. U.S.A.* **2000**, *97*, 3136−3141.
(49) Hernandez-Gil, J.; Llusar, S. F.; Maldonado, C. R.; Mareque-Rivas, J. C. *Chem. Commun.* **2011**, *47*, 2955−2957.
(50) Natale, D.; Mareque-Rivas, J. C. *Chem. Commun.* **2008**, 425−437.
(51) Stone, K. L.; Borovik, A. S. *Curr. Opin. Chem. Biol.* **2009**, *13*, 114−118.
(52) Shook, R. L.; Borovik, A. S. *Inorg. Chem.* **2010**, *49*, 3646−3660.
(53) Hart, J. S.; White, F. J.; Love, J. B. *Chem. Commun.* **2011**, *47*, 5711−5713.
(54) Kim, S.; Saracini, C.; Siegler, M. A.; Drichko, N.; Karlin, K. D. *Inorg. Chem.* **2012**, *51*, 12603−12605.
(55) Okamura, T.; Ushijima, Y.; Omi, Y.; Onitsuka, K. *Inorg. Chem.* **2013**, *52*, 381−394.
(56) Kövári, E.; Krämer, R. *J. Am. Chem. Soc.* **1996**, *118*, 12704−12709.
(57) Aït-Haddou, H.; Sumaoka, J.; Wiskur, S. L.; Folmer-Andersen, J. F.; Anslyn, E. V *Angew. Chem., Int. Ed.* **2002**, *41*, 4013−4016.
(58) Livieri, M.; Mancin, F.; Tonellato, U.; Chin, J. *Chem. Commun.* **2004**, 2862−2863.
(59) Livieri, M.; Mancin, F.; Saielli, G.; Chin, J.; Tonellato, U. *Chemistry* **2007**, *13*, 2246−2256.
(60) He, J.; Hu, P.; Wang, Y.-J.; Tong, M.-L.; Sun, H.; Mao, Z.-W.; Ji, L.-N. *Dalton Trans.* **2008**, 3207−3214.
(61) Bonomi, R.; Saielli, G.; Tonellato, U.; Scrimin, P.; Mancin, F. *J. Am. Chem. Soc.* **2009**, *131*, 11278−11279.
(62) Tjioe, L.; Joshi, T.; Forsyth, C. M.; Moubaraki, B.; Murray, K. S.; Brugger, J.; Graham, B.; Spiccia, L. *Inorg. Chem.* **2012**, *51*, 939−953.
(63) Tjioe, L.; Joshi, T.; Brugger, J.; Graham, B.; Spiccia, L. *Inorg. Chem.* **2010**, *50*, 621−635.
(64) Comba, P.; Gahan, L. R.; Hanson, G. R.; Westphal, M. *Chem. Commun.* **2012**, *48*, 9364−9366.
(65) Feng, G.; Mareque-Rivas, J. C.; Torres Martín de Rosales, R.; Williams, N. H. *J. Am. Chem. Soc.* **2005**, *127*, 13470−13471.
(66) Feng, G.; Mareque-Rivas, J. C.; Williams, N. H. *Chem. Commun.* **2006**, 1845−1847.
(67) Feng, G.; Natale, D.; Prabaharan, R.; Mareque-Rivas, J. C.; Williams, N. H. *Angew. Chem., Int. Ed.* **2006**, *45*, 7056−7059.
(68) Linjalahti, H.; Feng, G.; Mareque-Rivas, J. C.; Mikkola, S.; Williams, N. H. *J. Am. Chem. Soc.* **2008**, *130*, 4232−4233.
(69) Hernández-Gil, J.; Ferrer, S.; Salvador, E.; Calvo, J.; Garcia-España, E.; Mareque-Rivas, J. C. *Chem. Commun.* **2013**, *49*, 3655−3657.
(70) Carion, O.; Mahler, B.; Pons, T.; Dubertret, B. *Nat. Protoc.* **2007**, *2*, 2383−2390.
(71) Dubertret, B.; Skourides, P.; Norris, D. J.; Noireaux, V.; Brivanlou, A. H.; Libchaber, A. *Science* **2002**, *298*, 1759−1762.
(72) Gomez Blanco, N.; Jauregui-Osoro, M.; Cobaleda-Siles, M.; Maldonado, C. R.; Henriksen-Lacey, M.; Padro, D.; Clark, S.; Mareque-Rivas, J. C. *Chem. Commun.* **2012**, *48*, 4211−4213.
(73) *Bruker APEX2*. Bruker AXS, 2010.
(74) Sheldrick, G. M. *Acta Crystallogr., Sect. A* **2008**, *64*, 112−122.
(75) Wilson, A. J. C. *International Tables for Crystallography*; Kluwer Academic Publishers: Dordrecht, The Netherlands, 1995.
(76) Brandenburg, K.; Putz, H. DIAMOND. Crystal Impact GbR 2004.
(77) Cambridge Crystallographic Data Centre. http://www.ccdc.cam.ac.uk/pages/Home.aspx.
(78) Wilson, W.; Tanious, F.; Fernández-Saiz, M.; Rigl, C. In *Drug-DNA Interaction Protocols*; Fox, K. R., Ed.; Humana Press: New York, 1997; pp 219−240.
(79) Wilson, W. D.; Ratmeyer, L.; Zhao, M.; Strekowski, L.; Boykin, D. *Biochemistry* **1993**, *32*, 4098−4104.
(80) Strothkamp, K. G.; Stothkamp, R. E. *J. Chem. Educ.* **1994**, *71*, 77.
(81) Van den Berg, T. A.; Feringa, B. L.; Roelfes, G. *Chem. Commun.* **2007**, 180−182.
(82) Healy, P. C.; Engelhardt, L. M.; Patrick, V. A.; White, A. H. *J. Chem. Soc., Dalton Trans* **1985**, 2541.
(83) Zhang, Q.; Zhang, F.; Wang, W.; Wang, X. *J. Inorg. Biochem.* **2006**, *100*, 1344−1352.
(84) Aznar, E.; Ferrer, S.; Borrás, J.; Lloret, F.; Liu-González, M.; Rodríguez-Prieto, H.; García-Granda, S. *Eur. J. Inorg. Chem.* **2006**, *2006*, 5115−5125.
(85) Haasnoot, J. G. *Coord. Chem. Rev.* **2000**, *200*−*202*, 131−185.
(86) Klingele, M.; Brooker, S. *Coord. Chem. Rev.* **2003**, *241*, 119−132.
(87) Aromí, G.; Barrios, L. a.; Roubeau, O.; Gamez, P. *Coord. Chem. Rev.* **2011**, *255*, 485−546.
(88) Slangen, P. M.; van Koningsbruggen, P. J.; Goubitz, K.; Haasnoot, J. G.; Reedijk, J. *Inorg. Chem.* **1994**, *33*, 1121−1126.
(89) Ferrer, S.; van Koningsbruggen, P. J.; Haasnoot, J. G.; Reedijk, J.; Kooijman, H.; Spek, A. L.; Lezama, L.; Arif, A. M.; Miller, J. S. *J. Chem. Soc. Dalt. Trans* **1999**, 4269−4276.
(90) Prins, R.; Birker, P. J. M. W. L.; Haasnoot, J. G.; Verschoor, G. C.; Reedijk, J. *Inorg. Chem.* **1985**, *24*, 4128−4133.
(91) Yi, L.; Ding, B.; Zhao, B.; Cheng, P.; Liao, D.-Z.; Yan, S.-P.; Jiang, Z.-H. *Inorg. Chem.* **2004**, *43*, 33−43.
(92) Plass, W.; Pohlmann, A.; Subramanian, P. S.; Srinivas, D. *Z. Anorg. Allg. Chem.* **2002**, *628*, 1377.
(93) Patel, R. N.; Singh, N.; Shukla, K. K.; Gundla, V. L. N.; Chauhan, U. K. *J. Inorg. Biochem.* **2005**, *99*, 651−663.
(94) Morehouse, S. M. *Inorg. Chim. Acta* **1996**, *243*, 327−332.
(95) Haddad, M. S.; Duesler, E. N.; Hendrickson, D. N. *Inorg. Chem.* **1979**, *18*, 141−148.
(96) Strothkamp, K. G.; Lippard, S. J. *Acc. Chem. Res.* **1982**, *15*, 318−326.
(97) Haddad, M. S.; Hendrickson, D. N. *Inorg. Chem.* **1978**, *17*, 2622−2630.
(98) Kolks, G.; Lippard, S. J.; Waszczak, J. V.; Lilienthal, H. R. *J. Am. Chem. Soc.* **1982**, *104*, 717−725.
(99) Kolks, G.; Lippard, S. J. *J. Am. Chem. Soc.* **1977**, *99*, 5804−5806.
(100) Drew, M. G. B.; Martin Nelson, S.; Reedijk, J. *Inorg. Chim. Acta* **1982**, *64*, L189−L191.
(101) Verdejo, B.; Blasco, S.; García-España, E.; Lloret, F.; Gaviña, P.; Soriano, C.; Tatay, S.; Jiménez, H. R.; Doménech, A.; Latorre, J. *Dalton Trans.* **2007**, 4726−4737.
(102) Mota, A. J.; Rodríguez-Diéguez, A.; Palacios, M. A.; Herrera, J. M.; Luneau, D.; Colacio, E. *Inorg. Chem.* **2010**, *49*, 8986−8996.
(103) Suh, D.; Chaires, J. B. *Bioorg. Med. Chem.* **1995**, *3*, 723−728.
(104) Challis, G. L.; Hopwood, D. A.; Rappuoli, R.; Ulmer, J.; Palchaudhuri, R.; Hergenrother, P. J. *Curr. Opin. Biotechnol.* **2007**, *18*, 497−503.
(105) Boger, D. L.; Fink, B. E.; Brunette, S. R.; Tse, W. C.; Hedrick, M. P. *J. Am. Chem. Soc.* **2001**, *123*, 5878−5891.
(106) Cowan, J. A. *Curr. Opin. Chem. Biol.* **2001**, *5*, 634−642.
(107) Bazzicalupi, C.; Bencini, A.; Bonaccini, C.; Giorgi, C.; Gratteri, P.; Moro, S.; Palumbo, M.; Simionato, A.; Sgrignani, J.; Sissi, C.; Valtancoli, B. *Inorg. Chem.* **2008**, *47*, 5473−84.
(108) Itoh, T.; Hisada, H.; Sumiya, T.; Hosono, M.; Usui, Y.; Fujii, Y. *Chem. Commun.* **1997**, 677−678.
(109) An, Y.; Tong, M.-L.; Ji, L.-N.; Mao, Z.-W. *Dalton Trans.* **2006**, 2066−2071.
(110) Hegg, E. L.; Burstyn, J. N. *Inorg. Chem.* **1996**, *35*, 7474−7481.
(111) Deck, K. M.; Tseng, T. A.; Burstyn, J. N. *Inorg. Chem.* **2002**, *41*, 669−677.

(112) Hansma, H. G.; Revenko, I.; Kim, K.; Laney, D. E. *Nucleic Acids Res.* **1996**, *24*, 713−720.
(113) Moreno-Herrero, F.; Colchero, J.; Baró, A. M. *Ultramicroscopy* **2003**, *96*, 167−174.
(114) Lyubchenko, Y. L. *Proc. Natl. Acad. Sci. U.S.A.* **1997**, *94*, 496−501.
(115) Kornberg, R. D. *Science* **1974**, *184*, 868−871.
(116) Dabbousi, B. O.; Rodriguez-Viejo, J.; Mikulec, F. V.; Heine, J. R.; Mattoussi, H.; Ober, R.; Jensen, K. F.; Bawendi, M. G. *J. Phys. Chem. B* **1997**, *101*, 9463−9475.
(117) Isarov, A. V.; Chrysochoos, J. *Langmuir* **1997**, *13*, 3142−3149.
(118) Chan, Y.-H.; Chen, J.; Liu, Q.; Wark, S. E.; Son, D. H.; Batteas, J. D. *Anal. Chem.* **2010**, *82*, 3671−3678.
(119) Smith, A. M.; Nie, S. *J. Am. Chem. Soc.* **2008**, *130*, 11278−11279.

dx.doi.org/10.1021/ic4027249 | *Inorg. Chem.* 2014, 53, 578−593